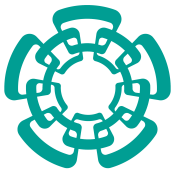

CENTER OF RESEARCH AND ADVANCED STUDIES OF NATIONAL POLYTECHNIC INSTITUTE

Zacatenco Campus

UMI-LAFMIA 3175 CNRS-CINVESTAV

"Modeling, Control and Development of a Quad Rotor Tail-Sitter VTOL-UAV"

THESIS

Presented by

Audwin Jean-baptiste

For the degree of

Master of Sciences

IN SPECIALTY OF

Autonomous Navigation of Aerial and Submarine Systems

Thesis Advisor:

Dr. Rogelio Lozano Leal

México, D.F. **June 2016**

Thesis Advisor and Chairman of Department
Dr.Rogelio Lozano Leal

Thesis Reader Dr. Salazar Cruz Sergio Rosario

Thesis Reader Dr.Colunga Gerardo Ramón Flores

Thesis Reader Dr. Osorio Cordero Antonio

I believe in intuition and inspiration. Imagination is more important than knowledge. For knowledge is limited, whereas imagination embraces the entire world, stimulating progress, giving birth to evolution. It is, strictly speaking, a real factor in scientific research. - Albert Einstein

Acknowledgments

Firstly, I am grateful to God for the good health and well being that were necessary to complete this thesis, and I am also thankful to my Mother **Anna Eugene Jean-baptiste**, my brothers for their supports and valuable guidance, encouragement extended to me during all my life.

Secondly, I would like to express my sincere gratitude to my advisors Dr. **Rogelio Lozano Leal**, specially to Dr. **Gerardo Flores Colunga**, for the continuous support of my M.S study and related research, for his patience, motivation, and immense knowledge. His guidance helped me in all the time of research and writing of this thesis. Besides my advisors, I would like to thank the rest of my thesis committee for their insightful comments and encouragement, but also for the hard question which incented me to widen my research from various perspectives. My sincere thanks also goes to Dr. **Sergio Salazar**, who provided me an opportunity to reach my objective, and who gave access to the laboratory and research facilities. Without his precious support it would not be possible to conduct this research. In particular, I am grateful to Dr. **Eduardo Steed Espinoza** for enlightening me the first glance of research. I thank my fellow labmates in for the stimulating discussions, for the sleepless nights we were working together, and for all the fun we have had in the last 2 years.

Finally, I would like to express my sincere thanks to CONACYT for the scholarships support during the last 2 years. Needless to say that there were times of hard feeling

and war of words too. But it only taught me to be more patient, considerate and shaped me to face the more difficult challenges in future

ABSTRACT

This thesis tackles the challenges of the design, development, modeling and control of a Quad Rotor Tail-Sitter VTOL Unmanned Aerial Vehicle (UAV) which connects the benefits of two different types of vehicles: fixed-wing and rotary-wing UAV's. Related to the goal of this thesis, Solidworks and XFLR5 are used to get an understanding, approximation analysis of the control allocation and modeling of the static forces and moments acting on the system.

A backstepping approach is used to control the flight path angle of the vehicle, considering the nonlinear nature of the lift force. The nonlinear controller designed makes the system reach the desired reference in flight path angle. A global stabilizing control law is derived which is valid for all the flight path angle envelope, since it is based on a general nonlinear model. A novel controller also presented in this work, by considering the rigid body dynamics, the controller operates in quaternions to avoid singularities, that are presented at some angular points. It also ensures a global stability of the vehicle in its envelope flight and it allows the autonomous transition of the system without discontinuities and switching signal for the overall system behavior.

Table of Contents

List of Figures

List of Tables

Chapter 1

Introduction

1.1 Background

Unmanned Aerial Vehicles (UAVs) have been employed successfully to address a large variety applications for many years, and are getting more useful nowadays by diverse and practicable applications, including advancements in aerodynamics, computers, and sensor technologies, which allow the aircraft to be used increasingly in different tasks. To refer a few, it is important recalling some applications in the area of surveillance [2], environmental awareness [3], search and rescue operations [4], aerial robotics [5]. As these tasks get more diversified, aircraft need to be continually adapted in order to perform multiple applications efficiently with a single air-frame. Picking a flight platform envelops many compromises, typically aircraft are classified as conventional aircraft or rotor craft. Normally, these classifications are chosen depending on the assigned mission.

Typically fixed wing (conventional) aircraft have high speeds and are capable of long flight times (good endurance), but they require large open areas (runways) for takeoff, landing or similar tasks. However rotor craft are capable to perform vertical takeoff and landing (VTOL) flight without the need of runways, special launch and recovery equipment, but they are limited in endurance and speed. There have been numerous

different methods of mixing these two styles of aircraft into a single air-frame, which provides the most effective design. The design, analysis, control, and construction of a Convertible UAV presents some arduous challenges, however these challenges are caused by the configuration of the vehicle but they are not insuperable.

1.1.1 Air-frame Configuration

The air-frame configuration is the most important part of UAV's development and contains all the hardware and software settings for the air-frame. It describes what hardware is required and which firmware, sensors, algorithms, etc. In the early 1950s the development of full scale VTOL aircraft and several air-frame configurations have been implemented over the years. A range of air-frame configuration is presented in [6], which is available for UAV, by their method of take-off and landing, it is accessible to set configurations into three appropriate types. These types are **HTOL** for aircraft which are required to accelerate horizontally along runway or trip in order to achieve flight speed. **VTOL**, these types of aircraft are those that can perform a maneuver of takeoff and landing vertically. These configurations will be explained with more details in this work, it is worth to say that, those three types of configurations can be divided into a large class of aircraft:

a) HTOL horizontal take-off and landing.

b) VTOL vertical take-off and landing.

c) Hybrids which attempt to combine the attributes of both these types.

1.1.2 UAV's Classification

UAVs can be classified by a wide types of features. As a numerous types of UAVs have beeng developed and tested in the early years, there is a challenge of classifying the new UAVs also it is laborious to develop a classification system that encompasses all of the categories of UAVs, because of their large useful applications. In this work a simple classification will be shown by taking each configuration of different UAVs, illustrating their own unique pros and cons. These characteristics which presently leads to the operator's decision in which platform will fit best for the application. UAVs aircraft currently boil down to two categories, fixed wing and rotary wing. As you may have guessed each of these categories can be further broken down, for instance a fixed wing UAV can be high wing, mid wing, low wing and flying wing, on the other hand rotary wing can be divided in Helicopter, Cyclogyro/Cyclocopter, Autogyro, Gyrodyne, Rotor kite, etc. UAV classification is usually determined by some criteria or features: shapes, application, range, altitude, endurance, speed, vehicle type, size. That distinguish several types of UAVs given rise to useful classification systems.

Fixed-Win use a set of stationary wings to generate lift and achieve flight, this kind of air-craft has a predetermined airfoil, which makes flight realizable by generating lift caused by the UAV's forward airspeed. This airspeed is generated by forward thrust usually by the means of a propeller being turned by an internal combustion engine or an electric motor. The control of a fixed-wing is produced by the control surfaces built into the wing itself, normally those consist of ailerons, elevators and a rudder. Which allow the fixed-wing to freely rotate around three axes that are perpendicular to each other and intersect at the UAV's center of gravity.

Fig. 1.1: RS-16 Fixed Wing UAV (American Aerospace)

Rotary Wings consist of 2 or more rotor blades that revolve around a fixed mass, this is known as a rotor. It also come in wide range of setups as well as more unusual like 12 and 16 rotor: one rotor or helicopter, two rotors tandem, three rotors tricopter, four rotors quadcopter, six rotor hexacopter, eight rotors octocopter. Like fixed wing solutions, these setups can be further broken down. For example the Y6 setup which consists of a tricopter with twin rotors on each arm, one pointing upwards and one pointing downwards, the X8, consists of a quadcopter with twin motors on each arm. Again each setup has their own unique characteristic advantages and disadvantages.

Fig. 1.2: UAV NEO 600 V2 Quadcopter

Free-Wing introduces a unique form of thrust-vectoring that creates a fundamentally new form of flight, an aircraft that is stable in all flight modes, from full hover through high-speed horizontal flight, even during transitions. The Free-wing Tilt-Body consist of two innovations in one air-frame. In a brief description, the wing is placed on bearings so that it is completely free to rotate in pitch. The fuselage itself is a lifting body, so the result is a left/right wing pair conjoined by a cross spar passing through the lifting body. Both the left/right wing pair and the central lifting body are free to rotate about the span-wise shaft, free with regard to the relative wind and free with regard to each other. [7].

Fig. 1.3: Freewing Scorpion UAV

Tilt-Wing has the special design concept that joins two completely different aircraft types, it combines of the advantages of a common fixed-wing aircraft, regarding flight performance and energy consumption, with the vertical take-off and landing (VTOL) capabilities of a rotary-wing configuration [8]. But it never became a viable rotating-wing concept to replace or surpass the capabilities of the helicopter. The idea is that the wing can be titled from its normal flying position with the propellers providing forward thrust, to a vertical position with the propellers providing vertical lift [7].

Fig. 1.4: Tilt-Wing (QTW, Chiba University)

Tilt-Rotor UAV combines the advantages of vertical takeoff and landing capabilities, inherent to the helicopter, with the rotors oriented like a helicopter [9]. With forward flight, the wing tip-mounted rotors are progressively titled to convert the aircraft into something that looks like a fixed-wing turboprop airplane. In this mode the tilt-rotor is able to achieve a considerably higher flight speed and endurance than those of an helicopter. This class of vehicle can be operated as a helicopter as well as a common fixed-wing, which means the aircraft has the capabilities to switch between Hover-to-Level and Level-to-Hover flights [7].

Fig. 1.5: Eagle Eye UAV (US Army)

The Tail-Sitter is a type of VTOL aircraft that employs a configuration that appears fairly conventional. Nevertheless, as the name insinuates, the aircraft is designed to perform a unique flight profile of hover-to-level and level-to-hover, while using the its tail for takeoff and landing. The same engine is used for both vertical and horizontal flight, it is the simplest way for the VTOL maneuver since it does not need extra actuators. Tail-Sitter has the ability to generate lift while in horizontal flight due to its conventional wings which gives to the vehicle an added value, for a more efficient forward flight, improved range, and longer loiter time than a conventional helicopter. The tail-sitter design was used in several prototypes in the early 50's, these include the Lockheed XFV-1, and the Ryan X-13 Vertijet. These aircraft were built and tested but never put into production [10].

Fig. 1.6: Sikorsky's Rotor Blown Wing UAV (DARPA'S VTOL)

1.1.3 Convertible UAV's Classification

Fixed wing conventional and hovering rotary-wing aircraft systems are the most commonly used. A relatively unexplored configuration is the convertible UAV tail-sitter,

due to the inelegant position during takeoff, hover and landing phases [11]. Generally convertible UAVs can be classified in three main classes:

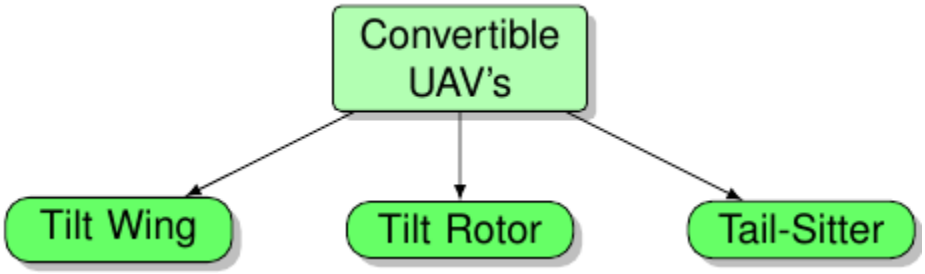

Fig. 1.7: Convertible Classification

Each of them can be sub-classified into a few sub-categories, which can be determined by the transition mechanism and air-frame configuration. Starting from Tilt-Wing and Tilt-Rotor, they can be categorized in convertiplane, which is a type of a convertible aerial vehicle that takes off, cruises, hovers and lands with the aircrafts reference line remaining horizontal (the main body configuration does not change during flight) [12]. There are some differences between of convertible aircraft, those of high-speed forward flight ability, most of those convertible aircraft involve tilting propellers such as manned aircrafts AV-8B Harrier[13], the new F-35 [14] and the V-22 Osprey which has two tilting jet engines to perform the transition [15], these aircrafts were designed for specific environment mission. Unfortunately these aircrafts, are not suitable for civilian's use and rescue operations. Moreover, such VTOL aircrafts, are less efficient in hover than a conventional helicopter or a tilting-rotor aircraft of the same gross weight [7]. Further the tilting mechanisms and control hardware increase the weight of the aircraft.

Alternatively, there has been a favorable interest, on performing the tail-sitter design in the mid twentieth century, this configuration not only has the takeoff and landing

vertical flight but also has the flight forward with high speed. Nowadays in recent research in unmanned vehicles, the tail-sitter has become a successfully platform and numerous different configuration of airframe have been developed as well as the T-Wing, which is one the most aged platform, shuch as: the T-wing was developed by the University of Sydney, which has a canard wing and tandem rotors [16], wile Jane's all the world's aircraft developed the Convair XF-Y1 tail-sitter [17], and US Air Force Research Lab and AeroVironment Inc. developed SkyTote which is equipped with a coaxial contra-rotating propeller [18]. Several successful tail-sitter UAV designs have been instrumented in the last years, the table shows some recent designs of tail-sitter that have been implemented in the recent years, illustrating the model, wingspan, weight, and propulsion.

Tail-Sitter List				
Manufacturer	**Model**	**Winspan**	**Weight**	**Propulsion**
Boeing	Heliwing	5.2 m	544 kg	Single turbojet turning two propellers
University of Sidney	Twing	2.13 m	29.5 kg	Twin 100cc gas motors and propellers
Aurora	Goldeneye 50	1.37 m	8.2 kg	Gas powered ducted fan
Aerovironment	Skytote	2.44 m	113.4 kg	Gas coaxial counter rotating propellers
MLB Company	V-Bat	1.52 m	22.7 kg	Gas powered ducted propeller
SUPAERO	Vertigo	0.65 m	1.6 kg	Electric coaxial counter-rotating propellers
Naval Postgraduate School	Archytas	4.27 m	45.4 kg	Electric coaxial counterrotating propellers
University of Arizona	Mini Vertigo	0.37 m	0.4 kg	Gas-powered ducted propeller

Table 1.1: Different Types of Tail-Sitter

1.1.4 Motivation

The development of unconventional miniature tail-sitter UAVs have made major progress to the huge improvements to fulfill the need in research area for a multi-objective. A miniature UAV design could be used to a number of fields, such as UAV fight control theories, electronic devices and material science. Unconventional miniature tail-sitter UAVs have great potential to use in diverse applications for many purposes in military and civilian operations, specially where there are severe constraint in the operating environment. These include, search and rescue, reconnaissance, border patrol, meteorological monitoring, wildfire tracking, etc.

1.1.5 Objectives

The objective of this project is to successfully modeling, control and development of a quad-rotor tail-sitter UAV by implementing the flight properties such as helicopter and airplane. So that the dynamics of the vehicle is divided into three modes of major flights:

- Helicopter Mode
- Airplane Mode
- Transition Mode, which is a transitional phase between the two aforementioned flight mode.

1. The objective of this work is firstly:

(a) Get the model of the Quad Rotor Tail-sitter UAV in its six degrees of freedom, for this purpose a similar vehicle as the Quadshot [19] has been used. For that purpose, the Quaternion and SO(3) have been studied.

(b) Design control laws to stabilize the vehicle in its three modes: hover, airplane, and transition. The last phase is the most complex presented, the major part of this project has been dedicated to this flight mode.

(c) Implement control laws in a previously designed platform using the autopilot PX4.

1.1.6 Contributions

Contributions from this project are divided in four sections. First, a significant design and analysis software proved to be a very useful tool for predicting the performance of a miniature tail-sitter UAV, such as Solidworks and XFLR5. Second, a mold is developed in fiberglass, for a fast production of vehicle and for a multiple reproductions. Third, two mathematical models are presented: one for the longitudinal flight and the other for the 6-DOF. Fourth, a control system is developed which allowed the air-plane to be completely controlled in vertical flight while flying both in and out of ground effect.

1.1.7 Summary

Having the benefit of a single air-frame that can be operated effectively in level and vertical flight, for that reason different kind of air-frame VTOL configurations are presented early, but for the goal of this work, the tail-sitter is chosen for further development.

Chapter 2

Modeling

2.1 Quaternion

Quaternion was first presented by William Rowan Hamilton in 1843 (19th-century) Irish mathematician, which can be applied to mechanics in three-dimensional space. Although the Euler angles represent a rotation by sequences rotating around three elements denoting **X**, **Y** or **Z** axes, quaternion also represents a rotation by a rotational angle around rotational axis, which is not necessary around the axes as considered in the Euler angles. Before presenting the properties of quaternion, let us define a striking feature of quaternion, is that, the product is noncommutative, which means that the product of two quaternions depends on which factor is to the left of the multiplication sign and which factor is to the right. Considering the standard orthogonal basis **i**, **j**, and **k** for the $\mathbb{R}^3$ vector in three dimensional space are written as a triplet of real numbers (scalar), thus the orthogonal basis are written as $\mathbf{i} = (1, 0, 0)$, $\mathbf{j} = (0, 1, 0)$, $\mathbf{k} = (0, 0, 1)$ that satisfy the next condition:

$$i^2 = j^2 = k^2 = ijk = -1 \tag{2.1}$$

A quaternion is a 4-tuple of real numbers *(hyper complex number)*, it defines an element

in $\mathbb{R}^4$, thus a quaternion can be represented by $q = (q_0, q_1, q_2, q_3)$ where q_0, q_1, q_2, and q_3 are simply real number or scalars, which can be defined as the sum of a scalar and a vector as follows

$$q = q_0 + iq_1 + jq_2 + kq_3 = q_0 + \mathbf{q} \tag{2.2}$$

where $\mathbf{q} = iq_1 + jq_2 + kq_3$ is the ordinary vector part in $\mathbb{R}^3$ and q_0 is the scalar part of the quaternion. Oftentimes in aerospace engineering, a special normalized quaternion is usually used such that $q_0 = cos(\frac{\alpha}{2})$, and $\mathbf{q} = \hat{e}sin(\frac{\alpha}{2})$, where $\hat{e}$ is represented the rotational axis, and α is the rotational angle.

The set of all quaternions with operations addition and multiplication can be defined a circle, in other word more explicitly a *non-commutative division circle*, which emphasizes that in the set of all quaternions every non-zero quaternion has an inverse and that quaternion products, in general, are *non-commutative*.

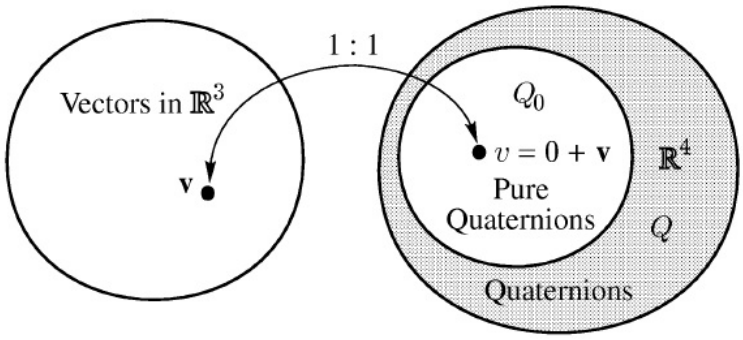

Fig. 2.1: Correspondence: Vector $\longleftrightarrow$ Quaternion[1]

As shown in fig.2.1, a *pure quaternion* can be defined as a quaternion, whose scalar part is zero. From one-to-one relationship between all vectors in $\mathbb{R}^3$ and their corresponding pure quaternion, the meaning of a product of a vector and a quaternion merely becomes the *quaternion* product of two quaternions, one of which is a pure quaternion [1], [20].

2.1.1 Quaternion and its properties

Equality and Addition

Let p be a quaternion, which can be defined as follow, $p = p_0 + ip_1 + jp_2 + kp_3$ and q is another quaternion, then the two quaternions are equal if only if $p_0 = q_0$, $p_1 = q_1$, $p_2 = q_2$, $p_3 = q_3$, that means they have the same rotational angle and the same rotational axis, for the special normalized quaternion used in aerospace engineering.

The sum of two quaternions is defined as follow, $p + q = (p_0 + q_0) + i(p_1 + q_2) + j(p_2 + q_2) + k(p_3 + q_3)$.

Multiplication and the Identity

As presented the standard basis in equation 2.1, which implicit in these equations

$$ij = i \times j = k = -j \times i = -ji \tag{2.3a}$$

$$jk = j \times k = i = -k \times j = -kj \tag{2.3b}$$

$$ki = k \times i = j = -i \times k = -ik \tag{2.3c}$$

having q and p defined as before, use 2.1, and 2.3. The quaternion algebra proceeds from these equations. The multiplication of two quaternions p and q is defined by:

$$p \otimes q = p_0 q_0 - \mathbf{p} \cdot \mathbf{q} + p_0 \mathbf{q} + q_0 \mathbf{p} + \mathbf{p} \times \mathbf{q} \tag{2.4}$$

In accordance with Hamiltons foregoing original equation, with the scalar part $p_0 q_0 - \mathbf{p} \cdot \mathbf{q}$

and the vector part $p_0\mathbf{q} + q_0\mathbf{p} + \mathbf{p} \times \mathbf{q}$, according to [20], the quaternion multiplicative identity has scalar part 1 and the vector part $(0, 0, 0)$. In the theory of the rotation sequences, quaternion multiplication can be used to represent two consecutive rotation. p and q are two quaternions, let them be the two consecutive rotations, where p represents the first rotation and q represents the second rotation, the composed rotation is given by $r = p \otimes q$.

Conjugate, Norm and Inverse

The complex conjugate of the quaternion q is denoted by

$$q^* = q_0 - \mathbf{q} = q_0 - iq_1 - jq_2 - kq_3 \tag{2.5}$$

it fallows that

$$(pq)^* = (p \otimes q)^* = q^* p^* = q^* \otimes p^* \tag{2.6}$$

it is also easy to verify the next operation

$$p + p^* = (q_0 + q) + (q_0 - q) = 2q_0 \tag{2.7}$$

the norm of a quaternion q is denoted as $\|q\| = \sqrt{q^* \otimes q}$ which can also be represented and it is easy to verify that the norm satisfies as fallows

$$\|q\| = \sqrt{q_0^2 + q_1^2 + q_2^2 + q_3^2} \tag{2.8}$$

By definition of an inverse we have $q^{-1}q = q^{-1} \otimes q = 1$, and $qq^{-1} = q \otimes q^{-1} = 1$ therefore we have $q^{-1} \otimes q = q \otimes q^{-1} = 1$

pre and post-multiplying by q^* gives $q^{-1}qq^* = q^{-1} \otimes q \otimes q^* = q^*$ and $q^*qq^{-1} = q^* \otimes q \otimes q^{-1} = q^*$ which can be represented by $q^{-1} \otimes q \otimes q^* = q^* \otimes q \otimes q^{-1} = q^*$.

Since $q^* \otimes q = q \otimes q^* = \|q\|^2$, if q is a unit quaternion, then

$$q^{-1} = \frac{q^*}{\|q\|^2} \tag{2.9a}$$

$$q^{-1} = q^* \tag{2.9b}$$

To conclude with the properties fo the quaternion, it is easy to see that the norm of the product of two quaternions p and q is the product of the individual norms because $\|p \otimes q\|^2 = (p \otimes q) \otimes (p \otimes q)^* = p \otimes q \otimes q^* \otimes p^*$

$$\|p \otimes q\|^2 = p \otimes \|q\|^2 \otimes p^* = p \otimes p^* \|q\|^2 = \|p\|^2 \|q\|^2. \tag{2.10}$$

2.1.2 Rotation by Quaternion Operator

First, we note that any unit quaternion (normalized quaternion) q may be written as $q = q_0 + \mathbf{q} = cos(\frac{\alpha}{2}) + \hat{e}sin(\frac{\alpha}{2})$. That is very clear to see that a quaternion does have the information about the rotational angle also the rotational axis. To be able to represent consecutive rotations, it is necessary to have the product of quaternions. Now let $p = cos(\frac{\beta}{2}) + \hat{e}sin(\frac{\alpha}{2})$ and $q = cos(\frac{\alpha}{2}) + \hat{e}sin(\frac{\alpha}{2})$ from 2.4, we get

$$r = p \otimes q = \left(cos\left(\frac{\beta}{2}\right) + \hat{e}sin\left(\frac{\beta}{2}\right)\right) \otimes \left(cos\left(\frac{\alpha}{2}\right) + \hat{e}sin\left(\frac{\alpha}{2}\right)\right)$$

$$r = cos\left(\frac{\beta}{2}\right) cos\left(\frac{\alpha}{2}\right) - \hat{e}sin\left(\frac{\beta}{2}\right) \cdot \hat{e}sin\left(\frac{\alpha}{2}\right) + cos\left(\frac{\beta}{2}\right) \hat{e}sin\left(\frac{\alpha}{2}\right)$$

$$+\hat{e}sin\left(\frac{\beta}{2}\right) cos\left(\frac{\alpha}{2}\right) + \hat{e}sin\left(\frac{\beta}{2}\right) \times \hat{e}sin\left(\frac{\alpha}{2}\right)$$

$$r = cos\left(\frac{\beta}{2}\right) cos\left(\frac{\alpha}{2}\right) - sin\left(\frac{\beta}{2}\right) sin\left(\frac{\alpha}{2}\right) + \hat{e}\left(sin\left(\frac{\beta}{2}\right) cos\left(\frac{\alpha}{2}\right) + cos\left(\frac{\beta}{2}\right) sin\left(\frac{\alpha}{2}\right)\right)$$

$$r = cos\left(\frac{\alpha+\beta}{2}\right) + \hat{e}sin\left(\frac{\alpha+\beta}{2}\right) = cos(\theta) + \hat{e}sin(\theta) \tag{2.11}$$

where $\hat{e}$ can be represented as $\hat{e} = \frac{\mathbf{q}}{\|\mathbf{q}\|}$ is the rotational axis and θ is represented as $\theta = tan^{-1}\left(\frac{\|\mathbf{q}\|}{q_0}\right)$ is the rotational angle. The previous equation 2.11, means that the product of two quaternions represents two consecutive rotations. For any unit quaternion and for any vector $\mathbf{v} \in \Re^3$, the action of a quaternion rotation operator involves multiplication of a quaternion and a vector, in consequence the multiplication of a quaternion and a vector should be defined. Suppose that the vector $\mathbf{v}$, is a pure quaternion which has the scalar part zero and the vector part $\mathbf{v}$, that means $v = 0 + \mathbf{v}$.

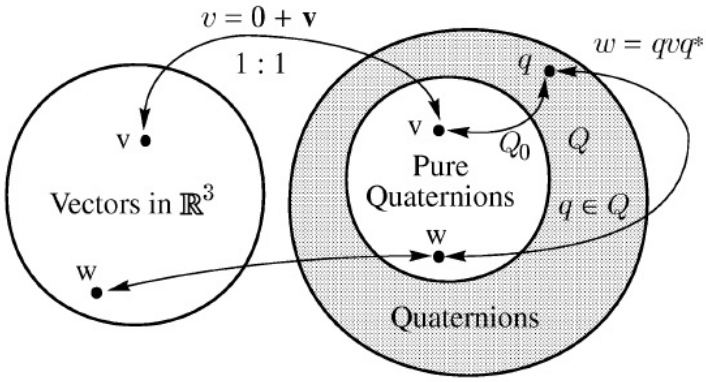

Fig. 2.2: Quaternion Operations on Vectors[1]

Consider v and $\mathbf{v}$ are interchangeable for both vector and pure quaternion. The multi-

plication of a vector and a quaternion is defined as:

$$q \otimes \mathbf{v} = (q_0 + \mathbf{q}) \otimes (0 + \mathbf{v}) = -\mathbf{q} \cdot \mathbf{v} + q_0\mathbf{v} + \mathbf{q} \times \mathbf{v} \tag{2.12}$$

The quartenion rotation operator takes $v \rightarrow \mathbf{w}$, let some notations are used for this purpose. Consider $\mathbf{a}$,$\mathbf{b}$ and $\mathbf{c}$ be any three dimensional vectors.

$$(\mathbf{a} \times \mathbf{b}) \times \mathbf{c} = (\mathbf{a} \cdot \mathbf{c})\,\mathbf{b} - (\mathbf{b} \cdot \mathbf{c})\,\mathbf{c} \tag{2.13a}$$

$$\mathbf{a} \times (\mathbf{b} \times \mathbf{c}) = (\mathbf{a} \cdot \mathbf{c})\,\mathbf{b} - (\mathbf{a} \cdot \mathbf{b})\,\mathbf{c} \tag{2.13b}$$

$$(\mathbf{a} \times \mathbf{b}) \cdot \mathbf{a} = (\mathbf{a} \times \mathbf{b}) \cdot \mathbf{b} = 0 \tag{2.13c}$$

Now using 2.12 and 2.13a, we obtain

$$\mathbf{w} = q \otimes \mathbf{v} \otimes q^* = (q_0 + \mathbf{q}) \otimes (0 + \mathbf{v}) \otimes (q_0\mathbf{q})$$

$$= (-\mathbf{q} \cdot \mathbf{v} + q_0\mathbf{v} + \mathbf{q} \times \mathbf{v}) \otimes (q_0 - \mathbf{q})$$

$$= -q_0\,(\mathbf{q} \cdot \mathbf{v}) + q_0\,(\mathbf{v} \cdot \mathbf{q}) + (\mathbf{q} \times \mathbf{v}) \cdot \mathbf{q} + (\mathbf{q} \cdot \mathbf{v})\,\mathbf{q} + q_0^2\mathbf{v} + q_0\,(\mathbf{q} \times \mathbf{v}) - q_0\,(\mathbf{v} \times \mathbf{q}) - (\mathbf{q} \times \mathbf{v}) \times \mathbf{q}$$

$$= (\mathbf{q} \cdot \mathbf{v})\,\mathbf{q} + q_0^2\mathbf{v} + 2q_0\,(\mathbf{q} \times \mathbf{v}) - (\mathbf{q} \cdot \mathbf{q})\,\mathbf{v} + (\mathbf{v} \cdot \mathbf{q})\,\mathbf{q}$$

$$= \left(2q_0^2 - 1\right)\mathbf{v} + 2\,(\mathbf{q} \cdot \mathbf{v})\,\mathbf{q} + 2q_0\,(\mathbf{q} \times \mathbf{v})$$

$$\mathbf{w} = \left(cos\left(\frac{\alpha}{2}\right) - sin^2\left(\frac{\alpha}{2}\right)\right)\mathbf{v} + 2\,(\mathbf{q} \cdot \mathbf{v})\,\mathbf{q} + 2q_0\,(\mathbf{q} \times \mathbf{v}) \tag{2.14}$$

Indeed, the quaternion operator can be represented explicitly by cosine matrix that

may be probably more helpful in some cases. From 2.14, considering

$$2(q_0^2-1)\mathbf{v} = \begin{bmatrix} (2q_0^2-1) & 0 & 0 \\ 0 & (2q_0^2-1) & 0 \\ 0 & 0 & (2q_0^2-1) \end{bmatrix} \begin{bmatrix} v_1 \\ v_2 \\ v_3 \end{bmatrix}$$

,

$$2(\mathbf{v}\cdot q)q = \begin{bmatrix} 2q_1^2 & 2q_1q_2 & 2q_1q_3 \\ 2q_1q_2 & 2q_2^2 & 2q_2q_3 \\ 2q_1q_3 & 2q_2q_3 & 2q_3^2 \end{bmatrix} \begin{bmatrix} v_1 \\ v_2 \\ v_3 \end{bmatrix}$$

,

$$2q_0(q\times\mathbf{v}) = \begin{bmatrix} 0 & -2q_0q_3 & 2q_0q_2 \\ 2q_0q_3 & 0 & -2q_0q_1 \\ 2q_0q_2 & 2q_0q_1 & 0 \end{bmatrix} \begin{bmatrix} v_1 \\ v_2 \\ v_3 \end{bmatrix}$$

,

we get

$$\begin{bmatrix} w_1 \\ w_2 \\ w_3 \end{bmatrix} = \begin{bmatrix} 2q_0^2-1+2q_1^2 & 2q_1q_2-2q_0q_3 & 2q_1q_3+2q_0q_2 \\ 2q_1q_2+2q_0q_3 & 2q_2^2+2q_0^2-1 & 2q_2q_3-2q_0q_1 \\ 2q_1q_3-2q_0q_2 & 2q_2q_3+2q_0q_1 & 2q_3^2+2q_0^2-1 \end{bmatrix} \begin{bmatrix} v_1 \\ v_2 \\ v_3 \end{bmatrix} \tag{2.15}$$

Notice that, it is worthy in view of 2.14,that 2.15 describes a complete rotation matrix bu using the Rodriguez formula, since they represented for quaternion rotation.

$$C = (q_0^2 - \mathbf{q}^T\mathbf{q})I + 2\mathbf{q}\mathbf{q}^T + 2q_0S(\mathbf{q}) \tag{2.16}$$

We just prove that $q \otimes \mathbf{v} \otimes q^*$, it is certainly the quaternion operator, which rotates $\mathbf{v}$ and α angle around $\hat{e}$. And it is a linear operator since, it holds the following relation,

$$q \otimes (k\mathbf{a} + \mathbf{b}) \otimes q^* = kq \otimes \mathbf{a} \otimes q^* \otimes \mathbf{b} \otimes q^* \tag{2.17}$$

that means for two vectors $\mathbf{a}$,$\mathbf{b}$, and a scalar k, for the prove of the equation 2.17, see [20],p 204. Related to the rotational matrix, the inverse of the operator $\mathbf{w} = q \otimes (\mathbf{v}) \otimes q^*$ on $\mathbf{v}$ is simple and it is given by

$$q^* \otimes (w) \otimes q = q^* \otimes (q \otimes (\mathbf{v}) \otimes q^*) \otimes q$$

$$= (q^* \otimes q) \otimes \mathbf{v} \otimes (q^* \otimes q) = \mathbf{v}$$

That rotates $\mathbf{w}$ an angle of α around $-q$ and brings $\mathbf{w}$ to $\mathbf{v}$. It is simple to prove that

$$\mathbf{v} = q^* \otimes \mathbf{w} \otimes q = (2q_0^2 - 1)\mathbf{w} + 2(q \cdot \mathbf{w})q - 2q_0(q \times \mathbf{w}) \tag{2.18}$$

we have

$$\begin{bmatrix} v_1 \\ v_2 \\ v_3 \end{bmatrix} = \begin{bmatrix} 2q_0^2 - 1 + 2q_1^2 & 2q_1q_2 + 2q_0q_3 & 2q_1q_3 - 2q_0q_2 \\ 2q_1q_2 - 2q_0q_3 & 2q_0^2 - 1 + 2q_2^2 & 2q_2q_3 + 2q_0q_1 \\ 2q_1q_3 + 2q_0q_2 & 2q_2q_3 - 2q_0q_1 & 2q_0^2 - 1 + 2q_3^2 \end{bmatrix} \begin{bmatrix} w_1 \\ w_2 \\ w_3 \end{bmatrix} \tag{2.19}$$

It is important to notice that, in view of (2.23), that (2.24) describes a complete rotation matrix bu using the Rodriguez formula as follow:

$$R = (q_0^2 - \mathbf{q}^T\mathbf{q})I + 2\mathbf{q}\mathbf{q}^T - 2q_0S(\mathbf{q}) \tag{2.20}$$

2.1.3 Matrix form of quaternion production

As we have already defined before in the equation 2.4, let $r = (r_0, r_1, r_2, r_3)$ which represented the composed quaternion of two consecutive quaternions.

$$r_0 = p_0q_0 - p_1q_1 - p_2q_2 - p_3q_3 \tag{2.21a}$$

$$r_1 = p_0q_1 + p_1q_0 + p_2q_3 - p_3q_2 \tag{2.21b}$$

$$r_2 = p_0q_2 - p_1q_3 + p_2q_0 + p_3q_1 \tag{2.21c}$$

$$r_3 = p_0q_3 + p_1q_2 - p_2q_1 + p_3q_0 \tag{2.21d}$$

It is important to note that quaternion multiplication is non-commutative, just as rotations are non-commutative[21].

$$\begin{bmatrix} r_0 \\ r_1 \\ r_2 \\ r_3 \end{bmatrix} = \begin{bmatrix} p_0 & -p_1 & -p_2 & -p_3 \\ p_1 & p_0 & -p_3 & p_2 \\ p_2 & p_3 & p_0 & -p_1 \\ p_3 & -p_2 & p_1 & p_0 \end{bmatrix} \begin{bmatrix} q_0 \\ q_1 \\ q_2 \\ q_3 \end{bmatrix} \tag{2.22a}$$

$$\begin{bmatrix} r_0 \\ r_1 \\ r_2 \\ r_3 \end{bmatrix} = \begin{bmatrix} q_0 & -q_1 & -q_2 & -q_3 \\ q_1 & q_0 & q_3 & -q_2 \\ q_2 & -q_3 & q_0 & q_1 \\ q_3 & q_2 & -q_1 & q_0 \end{bmatrix} \begin{bmatrix} p_0 \\ p_1 \\ p_2 \\ p_3 \end{bmatrix} \tag{2.22b}$$

2.1.4 Quaternion Derivative

Some algebraic manipulation are required, to represent the derivative of a quaternion. The time derivative of a unit quaternion it is the vector of *quaternion rates*, $\dot{q}$ are related to the angular velocity[22]. Let $q(t)$ represent the quaternion to a reference frame at time t, and $q(t + \triangle t)$ represent the quaternion to a reference frame at time $t + \triangle t$. $p(t) = cos\left(\frac{\triangle\alpha}{2}\right) + \hat{e}(t)sin\left(\frac{\triangle\alpha}{2}\right)$ be a quaternion that brings $q(t)$ to $q(t + \triangle t)$, which means, that $p(t)$ is an incremental quaternion with rotational axis $\hat{e}(t)$ and rotational angle $\triangle\alpha$[20].

For $\triangle\alpha \to 0$, $cos\left(\frac{\triangle\alpha}{2}\right) \to 1$ and $sin\left(\frac{\triangle\alpha}{2}\right) \to \frac{\triangle\alpha}{2}$, thus, $p(t) \approx 1 + \hat{e}(t)\frac{\triangle\alpha}{2}$

we have

$$q(t + \triangle t) = q(t) \otimes \left(1 + \hat{e}(t)\frac{\triangle t}{2}\right)$$

or

$$q(t + \triangle t) - q(t) = q(t) \otimes \left(0 + \hat{e}(t)\frac{\triangle t}{2}\right)$$

Divide $\triangle t$ at both side and let $\triangle t \to 0$, we get

$$\frac{dq}{dt} = q(t) \otimes \left(0 + \frac{1}{2}\hat{e}(t)\Omega(t)\right) = q(t) \otimes \left(0 + \frac{1}{2}\omega(t)\right)$$

where $\Omega(t) = \lim_{\triangle t \to 0} \frac{\triangle\alpha}{\triangle t}$ is a scalar, and $\omega(t) = \hat{e}(t)\Omega(t)$ is a vector, and $\left(0 + \frac{1}{2}\omega(t)\right)$

$= \frac{1}{2}\begin{pmatrix} 0 & \omega_1 & \omega_2 & \omega_3 \end{pmatrix}$ is a quaternion.

$$\begin{bmatrix} \dot{q}_0 \\ \dot{q}_1 \\ \dot{q}_2 \\ \dot{q}_3 \end{bmatrix} = \frac{1}{2}\begin{bmatrix} 0 & -\omega_1 & -\omega_2 & -\omega_3 \\ \omega_1 & 0 & \omega_3 & -\omega_2 \\ \omega_2 & -\omega_3 & 0 & \omega_1 \\ \omega_3 & \omega_2 & -\omega_1 & 0 \end{bmatrix}\begin{bmatrix} q_0 \\ q_1 \\ q_2 \\ q_3 \end{bmatrix} \tag{2.23a}$$

$$\begin{bmatrix} \dot{q}_0 \\ \dot{q}_1 \\ \dot{q}_2 \\ \dot{q}_3 \end{bmatrix} = \frac{1}{2}\begin{bmatrix} q_0 & -q_1 & -q_2 & -q_3 \\ q_1 & q_0 & -q_3 & q_2 \\ q_2 & q_3 & q_0 & -q_1 \\ q_3 & -q_2 & q_1 & q_0 \end{bmatrix}\begin{bmatrix} 0 \\ \omega_1 \\ \omega_2 \\ \omega_3 \end{bmatrix} \tag{2.23b}$$

2.2 Spacecraft Dynamics and Modeling

The quaternion based models have numerous benefits upon the Euler angle based models. For instance, the quaternion based model is uniquely defined because it does not depend on or *(need any)* rotational sequence, while a Euler angle based model can be different for different rotational sequences. Therefore, Euler angle based models may be error-prone if different groups of people are chosen to work on the same project but use different rotational sequences. Another attractive feature of quaternion based model is that a full quaternion model does not have any singular point in any rotational sequence. Which means quaternion determine any point on the sphere and include one *extra* coordinate which indicates the sense of rigid-body rotations. the are redundant as the poles of the sphere correspond to the same physical posture of the body yet, mathematically they used as two equilibria. But this brings especial difficulties to the

stability analysis of attitude-controlled rigid bodies.

From what has been discussed, in practice certain control actions cause the body rotate almost a full revolution to achieve a posture whichis close to the inertial one, i.e., to take the longer path. From an analytic of the view-point the two equilibria must be considered as different, hence one may not expect to achieve "global" stability properties in closed-loop. [23]. Therefore, quaternion model-based control design methods have been discussed in a number of literature. In [24] and [25] for precise definitions of stability and discussions.

In [26], Lyapunov function was used to design model-independent control law, model dependant control law, and adaptive control law. In [27] and [28], Lyapunov Functions were used to design control systems under the restriction of control input saturation. Though Lyapunov function is a powerful tool in global stability analysis, obtaining a control law and the associated Lyapunov function for the nonlinear systems is postulated by intuition, as noted in [29]. Moreover, most of these designs focus on the global stability and do not pay much attention on the performance of the control system. In [30], quaternion based linear error dynamics are adapted to get desired performance for the attitude control system using classical frequency domain methods, while in [31] an attitude control of a micro satellite by integrator backstepping based on quaternion feedback is presented, where the controller is shown to make the closed loop equilibrium points asymptotic stable in the sense of Lyapunov.

The inertial frame consists of $\mathbf{i}^i$ pointing north,$\mathbf{j}^i$ pointing east, and $\mathbf{k}^i$ pointing down and is centered at an arbitrary location. The origin of the body frame is at the center of gravity of the Vehicle and consists of $\mathbf{i}^b$ pointing out the nose of the aircraft, $\mathbf{j}^b$ pointing

out the right wing, and $\mathbf{k}^b$ pointing out the bottom of the aircraft.

2.2.1 Translational and Rotational Dynamics

It is relatively easy to study a rigid body in both kinematic and dynamics. Relating to the rigid body motion, focus on the chasles theorem in classical mechanics [32], any rigid motion can be totally decomposed without decoupling into a translation of the body about the mass center [33]. We presented both the translation and rotation for a rigid body w.r.t a fixed base coordinate frame.

Translational Dynamics

In [11] and [34], Newton's second law equation applied to translational motion of the aircraft takes the form:

$$f = m\frac{dV_g}{dt_i} \tag{2.24}$$

- The derivative of the right hand side of the equation 2.24 must be take with respect to inertial reference frame.
- f is the sum of all external forces.
- m is the mass of the aircraft.

Using the fact that

$$\frac{dV_g}{dt_i} = \frac{dV_g}{dt_b} + \omega_{b/i} \times V_g$$

performing the equation 2.24 by substituting the expression $\frac{dV_g}{dt_i}$, gives

$$f = \left(\frac{dV_g}{dt_b} + \omega_{b/i} \times V_g\right) m \tag{2.25}$$

expressing 2.25 in the body frame we have

$$f^b = \left(\frac{dV_g^b}{dt_b} + \omega_{b/i}^b \times V_g^b\right) m \tag{2.26}$$

where

$$V_g^b = \begin{pmatrix} u \\ v \\ w \end{pmatrix} \qquad \omega_{b/i}^b = \begin{pmatrix} p \\ q \\ r \end{pmatrix} \qquad f^b = \begin{pmatrix} f_x \\ f_y \\ f_z \end{pmatrix}$$

Hence $\frac{dV_g^b}{dt_b} = \begin{pmatrix} \dot{u} \\ \dot{v} \\ \dot{w} \end{pmatrix}$ we have the following expression

$$\begin{pmatrix} \dot{u} \\ \dot{v} \\ \dot{w} \end{pmatrix} = \begin{pmatrix} rv - qw \\ pw - ru \\ qu - pv \end{pmatrix} + \frac{1}{m} \begin{pmatrix} f_x \\ f_y \\ f_z \end{pmatrix} \tag{2.27}$$

For simplicity the equation 2.27 can be represented as

$$\dot{V}_g^b = -\omega_{b/i}^b \times V_g^b + \frac{1}{m} f^b \tag{2.28}$$

$$V = V_g^b$$

Rotational Dynamics

Applying Newton's second law to the rate of change of angular momentum of the rigid body, we have

$$M = \frac{dh}{dt_i} \tag{2.29}$$

- h is the angular momentum vector.
- M is the sum of all external moments.
- The derivative of the right hand side of the equation 2.2.1 taken w.r.t inertial frame.

Therefore we get

$$\frac{dh}{dt_i} = \frac{dh}{dt_b} + \omega_{b/i} \times h = M \tag{2.30}$$

expressing in the body frame therefore we have

$$\frac{dh^b}{dt_b} + \omega^b_{b/i} \times h^b = M^b \tag{2.31}$$

For a rigid body, angular momentum is defined as the product of the inertia matrix and the angular velocity vector:

$$h^b \triangleq J\omega^b_{b/i} \tag{2.32}$$

Let J be the inertia matrix of spacecraft defined by

$$J = \begin{bmatrix} J_{11} & J_{12} & J_{13} \\ J_{21} & J_{22} & J_{23} \\ J_{31} & J_{32} & J_{33} \end{bmatrix} \tag{2.33}$$

Diagonal elements are called moments of inertia. Off-diagonal elements are called products of inertia. J determined from mass properties in CAD program or measured experimentally using a bifilar pendulum. And J is a constant matrix, because it cannot change its values in the body frame.

$$J\frac{d\omega_{b/i}^{b}}{dt_b} + \omega_{b/i}^{b} \times \left(J\omega_{b/i}^{b}\right) = M^b \tag{2.34}$$

$$\frac{d\omega_{b/i}^{b}}{dt_b} = J^{-1}\left[-\omega_{b/i}^{b} \times \left(J\omega_{b/i}^{b}\right) + M^b\right] \tag{2.35}$$

The external moment M are principally composed of disturbance torque T_d due to gravitational, aerodynamic, solar radiation and many others environmental torques in the body frame, expressed by

$$T_d = [T_{d1}, \quad T_{d2}, \quad T_{d3}]^T \tag{2.36}$$

the control torque τ expressed by

$$\tau = [\tau_1, \quad \tau_2, \quad \tau_3]^T \tag{2.37}$$

Therefore, with $\omega = \omega^b_{b/i}$ we have

$$\dot{\omega} = J^{-1}\left[-\omega \times (J\omega) + T_d + \tau\right] \tag{2.38}$$

2.2.2 Kinematic Equation

Denoting the rotational axis of a body frame relative to a reference frame by a unit length vector $\hat{e}$ and the rotational angle by α, the scalar component of the quaternion $q_0 = cos\left(\frac{\alpha}{2}\right)$, the vector component of the quaternion $\mathbf{q} = \hat{e}sin\left(\frac{\alpha}{2}\right) = [q_1, \quad q_2, \quad q_3]^T$, then the quaternion that represents the rotation of the body frame relatively to the reference frame is expressed as follow:

$$q = \left[q_0, \, \mathbf{q}^T\right]^T = \left[cos\left(\frac{\alpha}{2}\right), \, \hat{e}sin\left(\frac{\alpha}{2}\right)\right]^T \tag{2.39}$$

the nonlinear spacecraft kinematics equations of motion can be represented by the quaternion

$$\begin{cases} \dot{\mathbf{q}} = & -\frac{1}{2}\omega \times \mathbf{q} + \frac{1}{2}q_0\omega \\ \dot{q}_0 = & -\frac{1}{2}\omega^T\mathbf{q} \end{cases} \tag{2.40}$$

It is worth mentioning that the kinematic quaternion equation can be represented in different form.

2.2.3 Kinematic and Dynamics of Rigid Body

In view of 2.23a and 2.23a the equation 2.40 can be written as

$$\dot{q} = \Omega(\omega)\, q \tag{2.41}$$

Using the 2.28, 2.38, 2.41 we obtain

$$\dot{P} = R(\mathbf{Q})\, V \tag{2.42a}$$

$$\dot{V} = -\omega \times V + \frac{1}{m} f \tag{2.42b}$$

$$\dot{\mathbf{Q}} = \Omega(\omega)\, \mathbf{Q} \tag{2.42c}$$

$$\dot{\omega} = J^{-1}\left[-\omega \times (J\omega) + M\right] \tag{2.42d}$$

- $P = [p_n \; p_e \; p_d]^T$ is the inertial frame position.
- $\mathbf{Q} = [q_0 \; q_1 \; q_2 \; q_3]^T$ is the quaternion representing the current attitude.
- $R(\mathbf{Q})$ is the rotation matrix from the body to the inertial frame.
- $V = [u \; v \; w]^T$ is the inertial velocity expressed in the body frame coordinates.
- m is the mass, f is the total external force applied.
- $\omega = [p \; q \; r]^T$ is the angular rates expressed in the body frame.
- J is the moment of inertia, and M is the net moment expressed in the body frame.

Chapter 3
Airfoil Analysis

3.1 Introduction

This chapter makes an analysis of the airfoil that has been used for the development of the aircraft, Although modern high-speed aircraft generally make use of advanced supercritical airfoil, there is still a demand for information on the NACA series of airfoil sections, which were developed over 50 years ago by the National Advisory Committee for Aeronautics. Computer programs were developed in the early 1970s to produce the ordinates for airfoils of any thickness, thickness distribution or camber in the NACA airfoil series.

3.1.1 Airfoil Geometry

The NACA airfoils were designed during the period from 1929 through 1947 under the direction of Eastman Jacobs at the NACAs Langley Field Laboratory. Most of the airfoils were based on simple geometrical descriptions of the section shape, although the 6 and 6A series were developed using theoretical analysis and do not have simple shape definitions. Although a new generation of airfoils has emerged as a result of improved understanding of airfoil performance and the ability to design new airfoils

using computer methods, the NACA airfoils are still useful in many aerodynamic design applications. A number of references have been included to allow the reader to study both the older NACA literature and the new airfoil design ideas. Taken together, this literature provides a means of obtaining a rather complete understanding of the ways in which airfoils can be shaped to obtain desired performance characteristics.

3.1.2 NACA 4 Digit Airfoil Specification

The NACA airfoils are constructed by mixing a thickness envelope with a camber or mean. In fact the NACA airfoil series is controlled by four digits, example NaCA 2411, which designate the camber, position of the maximum camber and thickness. As the NACA 2411 has beeen used, the next airfoil number is introduced: $NACA\ MPXX$. Although the numbering system implies integer values, the equations can provide 4 digit foils for arbitrary values of M, P, and XX.

- M is the maximum camber divided by 100. In the example $M = 2$ so the camber is 0.02 or 2% of the chord
- P is the position of the maximum camber divided by 10. In the example P=4 so the maximum camber is at 0.4 or 40% of the chord.
- XX is the thickness divided by 100. In the example $XX = 11$ so the thickness is 0.11 or 11% of the chord.

3.1.3 NACA 4 Digit Airfoil Calculation

The NACA airfoil section is created from a camber line and a thickness distribution plotted perpendicular to the camber line. The equation for the camber line is split into sections either side of the point of maximum camber position (P). In order to calculate the position of the final airfoil envelope later the gradient of the camber line is also required. The equations that describe this procedure are:

Camber Front $(0 \leq x < p)$

$$y_c = \frac{M}{P^2}\left(2Px - x^2\right) \tag{3.1}$$

Camber Back $(p \leq x \leq 1)$

$$y_c = \frac{M}{(1-P)^2}\left(1 - 2P + 2Px - x^2\right) \tag{3.2}$$

Gradient Front $(0 \leq x < p)$

$$\frac{dy_c}{dx} = \frac{2M}{P^2}\left(2P - x\right) \tag{3.3}$$

Gradient Back $(p \leq x \leq 1)$

$$\frac{dy_c}{dx} = \frac{2M}{(1-P)^2}\left(P - x\right) \tag{3.4}$$

The NACA 4 digit thickness distribution is given by

$$y_t = \frac{T}{0.2}\left(a_0 x^{0.5} + a_1 x + a_2 x^2 + a_3 x^3 + a_4 x^4\right) \tag{3.5}$$

$$a_0 = 0.2969 \qquad a_1 - 0.126$$

$$a_2 = -0.3516 \qquad a_3 = 0.2834$$

$$a_4 = -0.1015 \text{ or } -0.1036 \text{ for closed trailing edge.}$$

- The constants a_0 to a_4 are for a 20% thick airfoil. The expression $\frac{T}{0.2}$ adjusts the constants to the required thickness.
- At the trailing edge ($x = 1$) there is a finite thickness of 0.0021 chord width for a 20% airfoil. If a closed trailing edge is required the value of a_4 can be adjusted.
- The value of y_t is a half thickness and needs to be applied both sides of the camber line

Using the equations above, for a given value of x it is possible to calculate the camber line position y_c, the gradient of the camber line and the thickness. Which means, The NACA airfoils are constructed by combining a thickness envelope with a camber or mean line. Then the position of the upper and lower surface can be then calculated perpendicularly to the camber line.

$$\theta = atan\frac{dy_c}{dx}$$

Upper Surface:

$$x_u = x_c - y_t sin(\theta) \tag{3.6a}$$

$$y_u = y_c + y_t cos(\theta) \tag{3.6b}$$

Lower Surface:

$$x_l = x_c + y_t sin(\theta) \tag{3.7a}$$

$$y_l = y_c - y_t cos(\theta) \tag{3.7b}$$

The most obvious way to plot the airfoil is to iterate through equally spaced values of x calculating the upper and lower surface coordinates. While this works, the points are more widely spaced around the leading edge where the curvature is greatest and flat sections can be seen on the plots. To group the points at the ends of the airfoil sections a cosine spacing is used with uniform increments of β.
$x = \frac{1-cos(\beta)}{2}$ where $0 \leq \beta \leq \pi$.

3.1.4 NACA 4-Digit-Series Airfoils

The traditional NACA airfoil designations are shorthand codes representing the essential elements (such as thickness-chord ratio, camber, design lift coefficient) controlling the shape of a profile generated within a given airfoil type. Thus, for example the NACA 4-digit series airfoil is specified by a 4-digit code of the form pmxx, where p and m represent positions reserved for specification of the camber and xx allows for specification of the thickness-chord ratio as a percentage, that is, "pm12" designates a 12-percent-thick (t/c = 0.12) 4-digit airfoil. According to [35] Symmetric airfoils in the 4-digit-series family are designated by a 4-digit number of the form NACA 00xx. The first two digits indicate a symmetric airfoil; the second two, the thickness-chord ratio. Ordinates for the NACA 4-digit airfoil family [36] are described by an equation of the form:

$$\frac{y}{c} = a_0 \left(\frac{x}{c}\right)^{1/2} + a_1 \left(\frac{x}{c}\right) + a_2 \left(\frac{x}{c}\right)^2 + a_3 \left(\frac{x}{c}\right)^3 + a_4 \left(\frac{x}{c}\right)^4 \tag{3.8}$$

From the following boundary conditions the constant $\left(\frac{t}{c} = 0.20\right)$ were calculated in the equation.

Maximum Ordinate:

$$\frac{x}{c} = 0.30 \quad \frac{y}{c} = 0.10 \quad \frac{dy}{dx} = 0$$

Ordinate at Trailing Edge:

$$\frac{x}{c} = 1.0 \quad \frac{y}{c} = 0.002$$

magnitude of Trailing Edge Angle:

$$\frac{x}{c} = 1.0 \quad \left|\frac{dy}{dx}\right| = 0.234$$

Nose Shape:

$$\frac{x}{c} = 0.10 \quad \frac{y}{c} = 0.078$$

To obtain ordinates for airfoils in the family with a thickness other than 20 percent, the ordinates for the model with a thickness-chord ratio of 0.20 are multiplied by the ratio $(t/c)/0.20$. The leading-edge radius of this family is defined as the radius of curvature of the basic equation evaluated at $x/c = 0$. Because of the term $a_0(x/c)^{1/2}$ in the equation, the radius of curvature is finite at $x/c = 0$ and can be shown to be

$$R_{le} = \frac{a_0^2}{2} \left(\frac{t/c}{0.20}\right)^2 \tag{3.9}$$

by considering the limit as x approaches to zero of the standard expression for radius of curvature:

$$R = \frac{(1 + (dy/dx)^2)^{3/2}}{d^2y/dx^2} \tag{3.10}$$

The desired thickness-chord ratio is very important to the computer program to define an airfoil in this family. One might expect that this leading-edge radius $R(0)$, found in the limit as to depend only on the a_0 term of the defining equation, would also be the minimum radius on the profile curve. This is not true in general, for the NACA 0020 airfoil, for example, a slightly smaller radius ($R = 0.0435$ as compared to $R(0) = 0.044075$) is found in the vicinity of $x = 0.00025$

3.1.5 NACA 4-Digit-Modified-Series airfoils

The 4-digit-modified-series airfoils are designated by a 4-digit number followed by a dash and a 2-digit number (such as NACA 0012-63). The first two digits are zero for a symmetrical airfoil and the second two digits indicate the thickness-chord ratio. The first digit after the dash is a leading-edge-radius index number, and the second is the location of maximum thickness in tenths of chord aft of the leading edge. The design equation for the 4-digit-series airfoil family was modified [37] so that the same basic shape was retained but variations in leading-edge radius and chordwise location of maximum thickness could be made. Ordinates for these airfoils are determined from the following equations 3.10.

From the leading edge to the maximum thickness, and

$$\frac{y}{c} = d_0 + d_1\left(1 - \frac{x}{c}\right) + d_2\left(1 - \frac{x}{c}\right)^2 + d_3\left(1 - \frac{x}{c}\right)^3 \tag{3.11}$$

from the maximum thickness to trailing edge.

The constants in these equations can be calculated from the following boundary conditions (for $\frac{t}{c} = 0.20$):

Maximum Ordinate:

$$\frac{x}{c} = m \quad \frac{y}{c} = 0.10 \quad \frac{dy}{dx} = 0$$

Leading-Edge Radius:

$$\frac{x}{c} = 0 \quad R = \frac{a_0^2}{2}$$

Radius of curvature at maximum thickness:

$$R = \frac{(1-m)^2}{2d_1\,(1-m) - 0.588} \tag{3.12}$$

Ordinate at Trailing Edge:

$$\frac{x}{c} = 1.0 \quad \frac{dy}{dx} = d_0 = 0.002$$

Magnitude of Trailing-Edge Angle:

$$\frac{x}{c} = 1.0 \quad \frac{dy}{dx} = d_1 = f(m)$$

Then,the maximum ordinate, slope, and radius of curvature of the two portions of the surface match at $x/c = m$. The values of d_1 were chosen, as stated in [37], to avoid reversals of curvature and are given in the following table:

By using these constraints, equations were written for each of the constants (except a_0 and d_1) in the equation for the airfoil family and are included in the computer program. As in the 4-digit-series airfoil family, ordinates vary linearly with variations

m	d_1
0.2	0.200
0.3	0.234
0.4	0.135
0.5	0.465
0.6	0.700

Table 3.1: Reversal of Curvature

in thickness-chord ratio and any desired thickness shape can be obtained by scaling the design ordinates by the ratio of the desired thickness-chord ratio to the design thickness-chord ratio. The leading-edge index is an arbitrary number assigned to the leading-edge radius in reference 4 and is proportional to a_0. The relationship between leading-edge radius R_{le} and index number I is as follows:

$$R_{le} = 0.5 \left(0.2969 \frac{t/c}{0.2} \frac{I}{6} \right)^2 \tag{3.13}$$

Thus, an index of 0 indicates a sharp leading edge (radius of zero) and an index of 6 corresponds to $a_0 = 0.2969$, the normal design value for the 20 percent-thick 4-digit airfoil. A value of leading-edge index of 9 for a three times normal leading-edge radius was arbitrarily assigned in [37]

3.2 2D, 3D Analysis

For 2D, 3D analysis the application XFLR5 was used, this program was created by Mark Drela as a design tool for the Daedalus project at MIT (Massachusetts Institute of Technology) in the 80s. The XFLR5 allows us to analyze the profiles, wings, planes and airfoils, operating at low Reynolds numbers, and it facilitates the work with graphic

design. Application XFLR5 was used to calculate aerodynamic coefficients and stability metrics.

2D analysis is based on analyzing a NACA profile, then, using the so-called "Batch analisys", which allows us to obtain a polar curves, with these graphs and other data the analysis of complete airfoil can be studied.

3D analysis is the analysis of the wing or hydrofoil full rudder, with its endless profiles, and can also obtain polar and graphics. In short, it is not possible to work in 3D without going through 2D. That is, after making the analysis of the profiles (2D) is when we can work with the three dimensions (3D) to study the behavior of the plane, hydrofoil or airfoil. In this work the 3D analysis is not going to take into account, because a wing is set of several profiles, is like analyzing a set of profiles.

3.2.1 Reynolds Concept

The Reynolds number is a dimensionless quantity that lets us know when a fluid passes from laminar to turbulent flow. This number relates the density, viscosity, speed and a typical dimension in a dimensionless expression, which interpose in numerous problems of fluid dynamics. The Reynolds number is defined below.

$$Re = \frac{\rho \mathbf{v} L}{\mu} = \frac{\mathbf{v} L}{\nu} \tag{3.14}$$

where:

$\mathbf{v}$ is the maximum velocity of the object relative to the fluid (SI units: m/s).

L is a characteristic linear dimension, (travelled length of the fluid; hydraulic diameter

when dealing with river systems) (m).

μ is the dynamic viscosity of the fluid ($Pa \cdot s$ or $N \cdot s/m^2$ or $kg/(m \cdot s)$).

ν is the kinematic viscosity ($\nu = \mu/\rho)(m^2/s)$).

ρ is the density of the fluid (kg/m).

When choosing the profiles, the program indicates, at which point the boundary layer is clear and we can choose where that happens, besides being able to select whether the analysis takes into account the viscosity or not.

Normalized Reynolds

Most operations performed in XFLR5 are in Cartesian coordinates (X, Y). The coefficients CL, CD, CM are obtained by normalizing forces and moments with the dynamic pressure of the free stream *(the rope reference is supposed to be the unit)*. Similarly, the Reynolds number Re is defined by the velocity and viscosity of the free stream and involves rope unit:

$$C_L = \frac{L}{q} \quad , \quad C_D = \frac{D}{q}$$
$$C_M = \frac{M}{q} \quad , \quad \bar{q} = \frac{1}{2}\rho \mathbf{v}^2$$

The Reynolds number that used by XFLR5 in 2D profiles analysis and for the wind tunnels, experiences are always the same. For this dimensionless value, the rope reference is required, as for profiles is the rope and for wings is the aerodynamic mean chord.

Also in the engineering literature where it is necessary to calculate the values of frictional resistance (e.g. C_f vs Re for flat plate or tube) is often used the Reynolds number. Both Reynolds as the Mach number are dimensionless.

For the analysis of the profiles that were used in this project can be found in [19], since the idea of the first part of this work is based on the reconstruction of the vehicle mentioned in the cited reference with a rigid and very light materials such as carbon fiber.

3.3 Aerodynamic Forces

Almost all of aerial vehicles belong to two mainly classes fixed-wing vehicles, or rotary-wing vehicles. The first class is basically composed of airplanes. In this case, weight is compensated for by lift forces acting essentially on the wings, and propulsion is used to counteract drag forces associated with large air velocities. The second class contains several types of systems, like helicopters, ducted fans, quad-rotors, etc. In this case, lift forces are usually not preponderant and the thrust force, produced by one or several propellers, has also to compensate for the vehicle's weight.

There is a strong latent advantage on bringing control techniques related to airplanes an VTOLs. For the dependence of aerodynamic forces, there exist a major difficulty for the control of winged system, so-called *angle of attack*. To illustrates the usefulness concepts we focus on [38].

3.3.1 Background

Notation

- G represents the body's center of mas, m is the mas of the vehicle, and J is the vehicle's inertia matrix, both are assumed to be constant.

- $\mathcal{I} = \{\mathcal{O}; \vec{\imath}_o, \vec{\jmath}_o, \vec{k}_o\}$ is a fixed inertial frame with respect to (w.r.t) which the vehicle's absolute pose is measured. $\mathcal{B} = \{G; \vec{\imath}, \vec{\jmath}, \vec{k}\}$ is a frame attached to the body. The vector $veck$ is parallel to the thrust force axis. Which leaves two possibles and opposite directions for this vector the direction here can be chosen($\vec{k}$ pointing downward nominally) is consistent with the convention used for VTOL vehicles.

- The vector of coordinates of G in the fixed frame basis $\mathcal{I}$ can be denoted as $x = (x_1, x_2, x_3)^T$. Therefore, $\overrightarrow{OG} = \left(\vec{\imath}_o, \vec{\jmath}_o, \vec{k}_o\right) x$. The vector of coordinates associated with linear velocity of G w.r.t. $\mathcal{I}$ is denoted as $\dot{x} = (\dot{x}_1, \dot{x}_2, \dot{x}_3)^T$ and as $v = (v_1, v_2, v_3)^T$ when expressed in the basis of $\mathcal{B}$ which means $\frac{d}{dt}\overrightarrow{OG} = \vec{v} = \left(\vec{\imath}_o, \vec{\jmath}_o, \vec{k}_o\right) \dot{x} = \left(\vec{\imath}, \vec{\jmath}, \vec{k}\right) v$.

- The body-fixed frame orientation $\mathcal{B}$ w.r.t the inertial frame $\mathcal{I}$ can be represented by the rotation matrix R.The column vectors of R correspond to the vectors of coordinates of $\vec{\imath}, \quad \vec{\jmath}, \quad \vec{k}$ expressed in the basis of $\mathcal{I}$.

- The angular velocity vector of the body-fixed frame $\mathcal{B}$, relative to the fixed frame $\mathcal{I}$, expressed in $\mathcal{B}$ ca be denoted as $\omega = (\omega_1, \omega_2, \omega_3)^T$

- The fluid velocity w.r.t. the fixed frame $\mathcal{I}$ is denoted as $\vec{v}_f = \left(\vec{\imath}_o, \vec{\jmath}_o, \vec{k}_o\right) \dot{x}_f = \left(\vec{\imath}, \vec{\jmath}, \vec{k}\right) v_f$.

- The airspeed $\vec{v}_a$ of the body is the difference between the velocity of G and the fluid velocity, thus $\vec{v}_a = \vec{v} - \vec{v}_f$, with vector of coordinates is $\dot{x}_a \dot{x} - \dot{x}_f$ which expressed in the basis of the fixed frame $\mathcal{I}$, and $v_a = v - v_f$ which expressed in the basis of the fixed frame $\mathcal{B}$, which means $\vec{v}_a = \left(\vec{\imath}_o, \vec{\jmath}_o, \vec{k}_o\right) \dot{x}_a = \left(\vec{\imath}, \vec{\jmath}, \vec{k}\right) v_a$.

3.3.2 Modeling of Aerodynamic Forces

Lift and Drag Forces Models

To illustrate the models of lift and drag forces, we focus on [39], [40], a functional model of aerodynamic forces from [41] ruling the interactions between a solid body and the surrounding fluid is yonder the authors domain expertise, that spatial integration of these equations over the shape of an object does not yield closed-form expressions except in very specific cases. in spite of the delicate and complex issues associated with turbulent flows a side effect of which is the well known stall phenomenon for which no general complete theory exists to our knowledge. A different route has proposed by combining a well-accepted general expression of the intensity of aerodynamic forces with geometric considerations based on the body's symmetry properties. Let $\vec{F}_D$ and $\vec{F}_L$ represent the drag and lift components respectively of the $\vec{F}_a$

$$\vec{F}_a := \vec{F}_D + \vec{F}_L \tag{3.15}$$

by definition, $\vec{F}_L$ orthogonal to $\vec{v}_a$ and $\vec{F}_D$ parallel to $\vec{v}_a$. A pair of angle are also considered (α, β) which characterizing the orientation of $\vec{v}_a$ w.r.t the body frame. The *Buckingham* $\pi - theorem$ [42] asserts that the intensity of the static aerodynamic force varies like the square of the air speed $|\vec{v}_a|$ multiplied by a dimensionless function $C(\cdot)$ depending on the Reynolds number R_e , the Mach number M, and (α, β).

$$k_a := \frac{\rho \Sigma}{2}, \qquad |\vec{F}_a| = k_a |\vec{v}_a|^2 C\left(R_e, M, \alpha, \beta\right) \tag{3.16}$$

ρ the free stream air density, and Σ the area germane to the given body shape. Then, assuming that the direction of $\vec{F_a}$ depends upon the airspeed magnitude $|\vec{v}_a|$ via the $C(\cdot)$ function variables (R_e, M) only and that, this force does not depend(s) upon the angular velocity $\vec{\omega}$, this theorem in turn implies the existence of two dimensionless functions $C_D(\cdot)$ and $C_L(\cdot)$, and of a unit vector-valued function $\vec{r}(\cdot)$ characterizing the direction of the lift force w.r.t the body frame:

$$|\vec{F_L}| = k_a|\vec{v}_a|C_L\left(R_e, M, \alpha, \beta\right)\vec{r}\left(\alpha, \beta\right) \times \vec{v}_a \tag{3.17a}$$

$$|\vec{F_D}| = -k_a|\vec{v}_a|C_D\left(R_e, M, \alpha, \beta\right)\vec{v}_a \tag{3.17b}$$

$$\vec{r}\left(\alpha, \beta\right) \cdot \vec{v}_a = 0 \tag{3.17c}$$

In literature of aerodynamics $C_D(\in \mathbb{R}^+)$ and $C_L(\in \mathbb{R})$ are called the *aerodynamic characteristics* of the body, and also the *drag coefficient and lift coefficient* respectively. In this work, our objective is to reach these aerodynamics coefficients, for that reason the **proposition 2** in the [39]. Which can be defined by

$$\begin{cases} C_D\left(\alpha\right) & = c_0 + 2c_1 sin^2\left(\alpha\right) \\ C_L\left(\alpha\right) & = c_1 sin\left(2\alpha\right) \end{cases} \tag{3.18}$$

with c_0 and c_1 two real number.

Chapter 4

Control Designs

The development and use of dynamical systems is very important in control Designs, and which describes the system by mathematical representations. These mathematical representations can be used in control designs to study the behavior of the systems. The goal of the control designs is to design a such control's law to control a system, so-called plant, a general idea of a system can be represented as in figure 5.1, so its controlled variable follows a desired control signal, which may be a constant or variable value, to be realizable a controller is designed, which monitors the output and compares it with the reference. The error signal is the difference between actual and desired output, is applied as feedback to the input of the system, to bring the actual output closer to the reference.

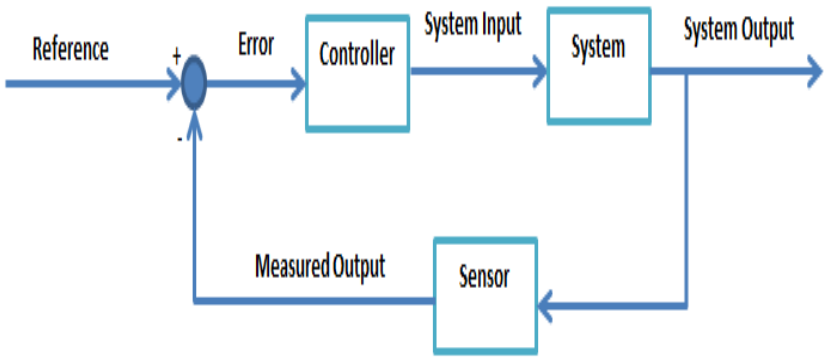

Fig. 4.1: Plant

4.1 Longitudinal Flight Dynamics Control

In many literature of flight dynamic, the flight control designs are considered that the aircraft dynamic to be linear at some point flight conditions such as [50]. This section discuss the problem of controlling a type of vehicle tail-sitter by exploring its nonlinearity dynamics. Therefore this section will be focus in a such control law that guarantee stability and can be reached a certain given reference. To achieve this objective the control technique back-stepping [51] will be applied and comparing to other control technique such as feedback linearization, back-stepping presents more flexible way to deal with the nonlinearity, a Lyapunov stability will be used to analyze the stability of the system. In [52] a contraction-based backstepping nonlinear control technique was proposed, which synthesis technique utilizes both the recursive nature of backstepping control and of contraction analysis and results in a contracting closed-loop dynamics, with exponential stability. While in [53] Backstepping controller is used for the construction of a globally stabilizing controller with a number of free parameters and implemented a controller with an internal loop controls involving the pitch rate of the aircraft and an external loop which includes angle of attack, path angle and pitch angle.

4.1.1 Aircraft Model

The equation of motion of the aircraft longitudinal dynamic take the form [54]

$$\dot{V_T} = \frac{1}{m}\left(F_T cos\alpha - D - mgsin\gamma\right) \tag{4.1a}$$

$$\dot{\alpha} = \frac{1}{mV_T}\left(-F_T sin\alpha - L + mgcos(\gamma)\right) + q \tag{4.1b}$$

$$\dot{\theta} = q \tag{4.1c}$$

$$\dot{q} = \frac{M\left(\delta_e\right)}{I_y} \tag{4.1d}$$

Let $\left[V_T\ \gamma\ \theta\ q\right]^T \in \mathbb{R}^4$ be the state vector, in this section the objective is to use the alternative model flight-path angle as a state variable in place of the angle of attack [55]. Where V_T is the aerodynamic speed, γ is the flight path angle, θ is the pitch angle, q is the pitch angular velocity. $\alpha = \theta - \gamma$ is the angle of attack, now let $\left[F_T\ \delta_e\right]^T \in \mathbb{R}^2$ be the control input vector, F_T is the engine thrust force, δ_e in our case represents the deflections of the control surfaces.

$$\dot{V_T} = \frac{1}{m}\left(-D + F_T cos\alpha - mgsin\gamma\right) \tag{4.2a}$$

$$\dot{\gamma} = \frac{1}{mV_T}\left(L + F_T sin\alpha - mgcos(\gamma)\right) \tag{4.2b}$$

$$\dot{\theta} = q \tag{4.2c}$$

$$\dot{q} = \frac{M\left(\delta_e\right)}{I_y} \tag{4.2d}$$

m and I_y are the mass and the inertia, while D, L and $M\left(\delta_e\right)$ are the aerodynamics forces lift, drag and pitch moment respectively as shown in the figure 5.2

In several literature the aerodynamic forces and moments are expressed by their non-

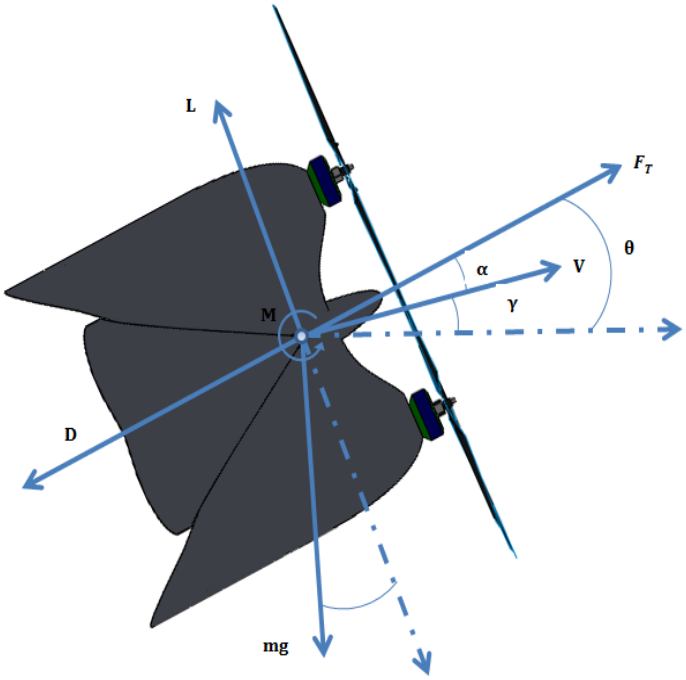

Fig. 4.2: Longitudinal Aircraft Illustration

dimensional coefficients, as follow:

$$L = \frac{1}{2}\rho V_T^2 S C_L, \qquad D = \frac{1}{2}\rho V_T^2 S C_D, \qquad M = \frac{1}{2}\rho V_T^2 S \bar{c} C_m \tag{4.3}$$

where ρ is the air density, S is the wing platform area, $\bar{c}$ is the mean aerodynamic chord and and C_L, C_D, C_m are the lift, drag and pitch moment coefficients, in [56] C_D, C_L can be expressed as:

$$C_D = C_{D_0} + k_1 C_L + k_2 C_L^2 \tag{4.4a}$$

$$C_m = C_{m_0} + \alpha C_{m_\alpha} + q C_{m_q} + \delta_e C_{m_\delta} \tag{4.4b}$$

C_{D_0}, k_1, k_2, C_{m_0}, C_{m_α} C_{m_q} and $C_{m_{\delta_e}}$ are the aircraft aerodynamic coefficients.

4.1.2 Flight Path Angle Control Design

The idea is based on the design for flight pah angle control, such as the system can seek a given reference γ_r

Assumption 1 *The following assumptions and simplification as illustrated in [57]:*

1. *The lift force coefficient, C_L, is assumed to be a function of α.*
2. *The time derivatives of the aircraft speed and altitude are neglected.*
3. *The flight path angle gamma,is assumed to be equal to the path angle reference γ_r, $\gamma = \gamma_r$ therefore $cos\gamma = cos\gamma_r$, this means $\dot{\gamma}$ is a function of $\alpha = \theta - \gamma$.*

For our objective a subsystem of the 5.2 was considered from 5.5a to 5.7b

$$\dot{\gamma} = \frac{1}{mV_T}\left(L\left(\alpha\right) + F_T sin\alpha - mgcos(\gamma_r)\right) \tag{4.5a}$$

$$\dot{\theta} = q \tag{4.5b}$$

$$\dot{q} = \frac{M\left(\delta_e\right)}{I_y} \tag{4.5c}$$

To achieve the objective of this control we have defined new variables such as the origin becomes the desired equilibrium point.

$$z_1 = \gamma - \gamma_r \tag{4.6a}$$

$$z_2 = \theta - (\gamma_r + \alpha_0) \tag{4.6b}$$

$$z_3 = q \tag{4.6c}$$

$$\psi(z_2 - z_2) = \psi(\alpha - \alpha_0) = \frac{1}{mV_T}(L(\alpha) + F_T sin\alpha - mgcos(\gamma_r))$$

through $\dot{\gamma} = \psi(0) = 0$, at the stable state the angle of attack is α_0, the function $(\alpha - \alpha_0)\psi(\alpha) > 0 \qquad \alpha \neq 0$. The equations 5.6a to 5.6c can be writing in their dynamic form:

$$\dot{z}_1 = \dot{\gamma} = \psi(z_2 - z_1) \tag{4.7a}$$

$$\dot{z}_2 = q = z_3 \tag{4.7b}$$

$$\dot{z}_3 = \dot{q} = u. \tag{4.7c}$$

The main idea of the change of variables is to make $z_2 = 0$, while it considered as a virtual control to stabilize $\dot{z}_1$, since it reached we have $\dot{z}_1 = \psi(-z_1)$

Step 1: Firstly, regarding the equation 5.7a is stabilized using the z_2 as the virtual control input. Introducing the control error 5.6a its derivation is given by

$$\dot{z}_1 = \psi(\alpha - \alpha_0) \tag{4.8}$$

by considering a constant reference value, now defining the Control Lyapunov Function (CLF)as:

$$W_1 = \frac{1}{2}z_1^2$$

now we determined the derivative of the (CFL) as follow

$$\dot{W}_1 = z_1 \dot{z}_1$$

$$\dot{W}_1 = z_1 \psi \left(\alpha - \alpha_0 \right) \Leftrightarrow z_1 \psi \left(z_2 - z_1 \right)$$

$$\dot{W}_1 = z_1 \psi \left(\theta - z_1 - \gamma_r - \alpha_0 \right)$$

$$\dot{W}_1 = z_1 \psi \left(- \left(1 + k_1 \right) z_1 + \theta - \gamma_r - \alpha_0 + k_1 z_1 \right)$$

To reach the stability of the subsystem we proposed a desired θ_d such as

$$\theta_d = \gamma_r + \alpha_0 - k_1 z_1 \tag{4.9}$$

hence $\dot{W}_1$ is negative definite $\forall \, k_1 > -1$

$$\dot{W}_1 = z_1 \psi \left(- \left(1 + k_1 \right) z_1 \right) \qquad z_1 \neq 0$$

Step 2: Now, let's introducing a new the variable from the equation 5.9.

$$z_2 = \theta - \theta_d = \theta - \gamma_r - \alpha_0 + k_1 z_1$$

For contentiousness a new variable has defined

$$\varsigma = - \left(1 + k_1 \right) z_1 + z_2$$

since the this variable has been defined, the equations 5.7a and 5.7b can be written as

$$\dot{z}_1 = \psi(\varsigma) \tag{4.10a}$$

$$\dot{z}_2 = k_1\psi + q \tag{4.10b}$$

Now extra term will be added to give an extra degree of freedom to the system $F(\varsigma)$ it must be positive definite and radially unbounded, this function was introduced in [58] to avoid the cancellation of term $\psi(\varsigma)$ for this reason a more flexible Lyapunov Function is consider by adding that function.

$$W_2 = k_2 W_1 + \frac{1}{2} z_2^2 + F(\varsigma)$$

Differentiating W_2 we obtain

$$\dot{W}_2 = k_2 z_1 \psi(\varsigma) + z_2 (q + k_1 \psi(\varsigma)) + F'(\varsigma)(-\psi(\varsigma) + q)$$

$$\dot{W}_2 = (k_2 z_1 + k_1 z_2 - F'(\varsigma))\psi(\varsigma) + (z_2 + F'(\varsigma))q \tag{4.11}$$

Now a new stabilizing function independently of $\psi(\varsigma)$ is required, taking

$$q_d = -k_3 z_2 \qquad k_3 > 0 \tag{4.12a}$$

$$F'(\varsigma) = k_4 \psi(\varsigma) \qquad F(0) \qquad k_4 > 0 \tag{4.12b}$$

then the equation 5.11 becomes

$$\dot{W}_2 = \left(k_2 z_1 + \left(k_1 - k_3 k_4\right) z_2\right) \psi\left(\varsigma\right) - k_4 \psi\left(\varsigma\right)^2 - k_3 z_2^2$$

the next variable has been proposed such as $\dot{W}_2$ can be negative definite

$$k_2 = -\left(1 + k_1\right)\left(k_1 - k_3 k_4\right) \qquad k_3 k_4 > k_1 \tag{4.13}$$

hence $\dot{W}_2$ becomes

$$\dot{W}_2 = -\left(k_1 - k_3 k_4\right) \varsigma \psi\left(\varsigma\right) - k_4 \psi\left(\varsigma\right)^2 - k_3 z_2^2$$

Step 3: Finally the third error is introduced

$$z_3 = q - q_d = q + k_3 z_2$$

updating the system description we obtained

$$\dot{z}_1 = \psi\left(\varsigma\right) \tag{4.14a}$$

$$\dot{z}_2 = z_3 - k_3 z_2 + k_1 \psi\left(\varsigma\right) \tag{4.14b}$$

$$\dot{z}_3 = u + k_3\left(z_3 - k_3 z_2 + k_1 \psi\left(\varsigma\right)\right) \tag{4.14c}$$

A new Lyapunov Function is introduced by introducing a penalizing term.

$$W_3 = k_5 W_2 + \frac{1}{2} z_3^2 \qquad k_5 > 0$$

the W_3 time derivative is computed.

$$\begin{aligned}\dot{W}_3 = & k_5\left(\left(k_1 - k_3k_4\right)\varsigma\psi\left(\varsigma\right) - k_4\psi\left(\varsigma\right)^2 - k_3z_2^2 + z_3\left(z_2 + k_4\psi\left(\varsigma\right)\right)\right) \\ & + z_3\left(u + k_3\left(z_3 - k_3z_2 + k_1\psi\left(\varsigma\right)\right)\right)\end{aligned}$$

$$\dot{W}_3 \leqslant -k_3k_5\psi^2\left(\varsigma\right) - k_3k_5z_2^2 + z_3\left(u + k_3z_3 + \left(k_5 - k_3^2\right)z_2 + \left(k_1k_3 + k_4k_5\right)\psi\left(\varsigma\right)\right)$$

to cancel the cross product we selected $k_5 = k_3^2$ we have

$$\dot{W}_3 \leqslant -k_3k_5\psi^2\left(\varsigma\right) - k_3k_5z_2^2 + z_3\left(u + k_3z_3 + \left(k_1k_3 + k_4k_5\right)\psi\left(\varsigma\right)\right)$$

Now the control input has proposed as fallow

$$u = -k_6z_3 = -k_6\left(q + k_3\left(\theta + k_1\left(\gamma - \gamma_r\right) - \gamma_r - \alpha_0\right)\right) \qquad k_6 > k_3 \tag{4.15}$$

such that $\dot{W}_3$ becomes negative definite and can be written as

$$\dot{W}_3 \leq -k_3^2k_4\psi^2\left(\varsigma\right) - k_3^3z_2^2 - \left(k_6 - k_3\right)z_3^2 + \left(k_1k_3 + k_3^2k_4\right)z_3\psi\left(\varsigma\right)$$

As we can see $\dot{W}_3$ is not completely negative definite as we expected, only the first three term on the right hand side are beneficial for this reason we complete it with the squares.

$$\dot{W}_3 \leq -k_3^3z_2^2 - \left(k_6 - k_3\right)\left(z_3 - \frac{k_1k_3 + k_3^2k_4}{2\left(k_6 - k_3\right)}\psi\left(\varsigma\right)\right)^2 - \left(z_3 - \frac{k_1k_3 + k_3^2k_4}{2\left(k_6 - k_3\right)}\right)\psi\left(\varsigma\right)^2$$

$\dot{W}_3$ becomes negative definite since $\psi^2\left(\varsigma\right)$ coefficient is negative, which can be proved

since.

$$k_6 > k_3 \left(1 + \frac{(k_1 + k_3 k_4)^2}{4 k_3 k_4}\right) \tag{4.16}$$

k_4 is chosen to minimize this lower limit under the constraints that $k_4 > 0$, $k_3 k_4 > k_1$ and for $k_1 \leq 0$, $(k_1 + k_3 k_4)$ is chosen arbitrarily small, hence the equations 5.16 becomes $k_6 > k_3$

Using the backstepping approach the system 5.5 changed into 5.14, by implementing an extra term and latter the control law has shown 5.15 to be globally stabilizing since the system presented a nonlinear nature.

4.1.3 Surface Deflection

This section is focus on the issue of reaching the control of surface deflections δ, which will produce the desired pitching moment M. Derivation of the control law that have been found in equation 5.15 is regarding the angular pitch acceleration $\dot{q}$ as a variable of control. As we have already demonstrated in 5.5c the control law can be represented as follow:

$$\dot{q} = u = \frac{M(\delta_e)}{I_y} \tag{4.17}$$

with the control law can be transformed into

$$I_y u = \beta \left(C_{m_0} + \alpha C_{m_\alpha} + q C_{m_q} + \delta_e C_{m_\delta}\right)$$

where $\beta = \frac{1}{2}\rho V_T^2 S_{\bar{c}}$ with that the control of surface deflection is obtained

$$\delta_e = \frac{1}{C_{m_\delta}} \left(\frac{I_y u}{\beta} - \left(C_{m_0} + \alpha C_{m_\alpha} + q C_{m_q}\right)\right) \tag{4.18}$$

4.2 Quaternion Based Trajectory Tracking Control

Regarding to the translational kinematic in equation 2.42, relative velocity and relative acceleration between rigid bodies in motion have introduced, and in particular the Coriolis acceleration. Considering the second subsystem in the equation 2.42, the attitude of a rigid body can be described by different representations, some of which are given in this section, and the attitude control consists in achieving any rigid-body orientation relative to a fixed frame, independently of that attached to the body itself. The best manner to explain the kinematics and dynamics is to consider the attitude of a satellite relative to the Earth.

4.2.1 Rotation Matrix

As in [59] a rotation matrix $\mathbf{R}$ describing the orientation of frame $\mathcal{F}_1$ with respect to frame $\mathcal{F}_2$ consists of the projection of the axes of $\mathcal{F}_1$ onto $\mathcal{F}_2$. The column vectors of $\mathbf{R}$ represent the coordinates of the axes of $\mathcal{F}_1$ described in $\mathcal{F}_2$. Since the axes of $\mathcal{F}_1$ and $\mathcal{F}_2$ are usually unit vectors, the rotation matrix contains only cosine terms and is called the direction cosine matrix. Also, since the axes of reference frames are orthonormal, the rotation matrix is orthogonal and belongs to the set

$$SO\left(3\right) := \{\mathbf{R} \in \mathbb{R}^{3x3} \mid det\left(\mathbf{R}\right) = 1, \mathbf{R}\mathbf{R}^T = \mathbf{R}^T\mathbf{R} = \mathbf{I}_3\} \tag{4.19}$$

Where $\mathbf{I}_3$ denotes the identity matrix and inverse $\mathbf{R}^{-1} = R^T$. The set $SO(3)$ give a unique and nonsigular representation of the attitude and generally referred to as the rotation space.

A rotation matrix is usually used to map vector coordinates from one frame to another frame. Let $\mathbf{R} \in SO(3)$ describe the rotation from frame $\mathcal{F}_1$ to frame $\mathcal{F}_2$. If the coordinates of a vector in $\mathcal{F}_1$ is denoted by $\mathbf{x}_1$, then the coordinates of this vector in frame $\mathcal{F}_2$ is denoted by $\mathbf{x}_2$, given by

$$\mathbf{x}_2 = R\mathbf{x}_1 \tag{4.20}$$

The above property can be applied to the case of several frames, leading to the composition of rotations, which is obtained by the noncommutative multiplication appropriate rotation matrices.

4.2.2 Axis-Angle Parameterization

The relative orientation of two reference frames can always be expressed by a single rotation about a given normalized vector by a given rotation angle. Let $\hat{e} \in \mathbf{R}^3$ denote a unit vector, and θ denote the angle of rotation about $\hat{e}$. Then the corresponding rotation matrix $R(\theta, \hat{e}) \in SO(3)$ is given by the following formula:

$$\mathbf{R}(\theta, \hat{e}) = \mathbf{I}_3 - \sin(\theta)\,\mathbf{S}(\hat{e}) + (1 - \cos(\theta))\,\mathbf{S}(\hat{e})^2 . \tag{4.21}$$

where $\mathbf{S(x)}$ is the skew symmetric matrix associated to $\mathbf{x} = [x_1,\, x_2,\, x_3]^T \in \mathbb{R}^3$ given by

$$\mathbf{S}(\mathbf{x}) = \begin{bmatrix} 0 & -x_3 & x_2 \\ x_3 & 0 & -x_1 \\ -x_2 & x_1 & 0 \end{bmatrix} \in \mathbb{R}^{3x3} \tag{4.22}$$

Satisfying $\mathbf{S}(\mathbf{x}) := \mathbf{x} \times \mathbf{y}$, where $\mathbf{x}, \mathbf{y}$, and the "$\times$" denotes the vector cross product.

4.2.3 Unit Quaternion

The unit quaternion is defined as a four-element representation of the attitude, denoted by

$$\mathbf{Q} = \begin{pmatrix} \mathbf{q} \\ \eta \end{pmatrix} \in \mathbb{Q} \tag{4.23}$$

where $\mathbf{q} \in \mathbb{R}^3$, $\eta \in \mathbb{R}$ and $\mathbb{Q}$ is set of unit quaternion represented as

$$\mathbb{Q} = \{\mathbf{Q} \in \mathbb{R}^4 \mid |\mathbf{Q}| = 1\} \tag{4.24}$$

The unit quaternion is usually considered as an axis representation. In fact the rotation by an angle θ about an arbitrary unit-length vector $\hat{e} \in \mathbb{R}^3$ can be described by the unit quaternion

$$\mathbf{Q} = \begin{pmatrix} \hat{e} \sin(\theta/2) \\ \cos(\theta/2) \end{pmatrix} \tag{4.25}$$

where $\eta = \cos(\theta/2) \in \mathbb{R}$ is the scalar part and $\mathbf{q} = \hat{e} \sin(\theta/2) \in \mathbb{R}^3$ is the vector part.

Through a transformation that provides a rotation matrix associated to the unit quaternion $\mathbf{Q}$, that brings the inertial frame into the body frame can be obtained through the Rodriguez formula as

$$\mathbf{R} = \left(\eta^2 - \mathbf{q}^T\mathbf{q}\right)\mathbf{I}_3 + 2\mathbf{q}\mathbf{q}^T - 2\eta\mathbf{S}\left(\mathbf{q}\right) \tag{4.26}$$

$\mathbb{Q}$ forms a group with quaternion multiplication, which is distributive and associative, but not commutative. To define this operation, consider two unit quaternion.

$$\mathbf{Q}_1 = \begin{pmatrix} \mathbf{q}_1 \\ \eta_1 \end{pmatrix},\ \mathbf{Q}_2 = \begin{pmatrix} \mathbf{q}_2 \\ \eta_2 \end{pmatrix}$$

The difference between two posture is given by the quaternion product, denoted by $\mathbf{Q}_1 \otimes \mathbf{Q}_2 \in \mathbb{Q}$

$$\mathbf{Q}_1 \otimes \mathbf{Q}_2 = \begin{pmatrix} \eta_1\mathbf{q}_2 + \eta_2\mathbf{q}_1 + \mathbf{S}\left(\mathbf{q}_1\right)\mathbf{q}_2 \\ \eta_1\eta_2 - \mathbf{q}_1^T\mathbf{q}_2 \end{pmatrix} \tag{4.27}$$

The multiplication of quaternion can be denoted by $\mathbf{Q}_1 \otimes \mathbf{Q}_2 = \mathbf{Q}_3$, and the rotation matrix associated to $\mathbf{Q}_3$ is obtained as $\mathbf{R}\left(\mathbf{Q}_3\right) = \mathbf{R}\left(\mathbf{Q}_2\right)\mathbf{R}\left(\mathbf{Q}_1\right)$. The inverse attitude is performed by the inverse conjugated

$$\bar{\mathbf{Q}} = \mathbf{Q}^{-1} = \left[-\mathbf{q}^T\ \eta\right]^T \in \mathbb{Q} \tag{4.28}$$

Recalling That $\mathbf{Q}$ and $-\mathbf{Q}$ represent the same physical attitude however, the two postures differ mathematically by 2π rotation an arbitrary axis. As a consequence, the mathematical model has two equilibria and this must be considered in stability study.

Rodrigues Parameters

The Rodrigues vector is another representation of the attitude and is derived from the definition of the unit quaternion $\mathbf{Q}$ in 5.25 as [60]

$$\varphi := \frac{1}{\eta}\mathbf{q} = \hat{e}\tan(\theta/2) \tag{4.29}$$

where the three elements of φ are known as the Rodrigues parameters. The rotation matrix relative to φ can be obtained from 5.26 as in [60]

$$\mathbf{Q} = \frac{1}{\sqrt{1+|\varphi|^2}}\begin{pmatrix}\varphi\\1\end{pmatrix} \tag{4.30}$$

The Rodrigues parameters representation uses only three elements and hence is minimal. However, the Rodrigues vector cannot be used to represent rotations through $\pm\pi$, which correspond to $\eta = 0$. A different but related representation to the Rodrigues parameters is the modified Rodrigues parameters (MRP) representation. The Modified Rodrigues parameters are the elements of the vector $\bar{\varphi}$ defined as

$$\bar{\varphi} := \frac{1}{1+\eta}\mathbf{q} = \hat{e}\tan(\theta/4) \tag{4.31}$$

The modified Rodrigues parameterization shares many characteristics with the rotation vector parametrization, including the occurrence of discontinuous jumps in the parameter space when incrementing the rotation.

It is clear that the MRP representation of the attitude is also minimal; however, the

modified Rodrigues vector is not defined for $\eta = -1$. This indicates that the singularity has moved to $\pm 2\pi$ as compared to the Rodrigues vector.

Kinematics and Dynamics Representation

The time derivative of the rotation matrix can be determined as

$$\dot{\mathbf{R}}(\mathbf{Q}) = -\mathbf{S}(\omega)\,\mathbf{R}(\mathbf{Q}) \tag{4.32}$$

where $\mathbf{S}(\cdot)$ is the skew symmetric matrix, for our purpose we represented the kinematic differential equation of the rigid body attitude as follow

$$\dot{\mathbf{Q}} = \frac{1}{2}\mathbf{T}(\mathbf{Q})\,\omega \tag{4.33}$$

Where $\mathbf{T}(\mathbf{Q})$ is given by

$$\mathbf{T}(\mathbf{Q}) = \begin{pmatrix} \eta\mathbf{I}_3 + \mathbf{S}(\mathbf{q}) \\ -\mathbf{q}^T \end{pmatrix} \tag{4.34}$$

Which satisfies $\mathbf{T}(\mathbf{Q})^T\,\mathbf{T}(\mathbf{Q}) = \mathbf{I}_3$, therefore, the inverse kinematic problem can be solved as

$$\omega = 2\mathbf{T}(\mathbf{Q})^T\,\dot{\mathbf{Q}} \tag{4.35}$$

Regarding the the rigid body model 2.42, the rotational Dynamics can be rewritten as

$$\dot{\mathbf{Q}} = \frac{1}{2}\mathbf{T}\left(\mathbf{Q}\right)\omega \tag{4.36a}$$

$$\mathbf{J}\dot{\omega} = \tau - \mathbf{S}\left(\omega\right)\mathbf{J}\omega \tag{4.36b}$$

4.2.4 Quaternion Attitude Error Dynamics

The attitude control goal is based on making the actual attitude converge towards to the unit quaternion representing the desired attitude of the vehicle $\mathbf{Q}_d$, which satisfying the kinematic equation.

$$\dot{\mathbf{Q}} = \mathbf{T}\left(\mathbf{Q}_d\right)\omega_d \tag{4.37}$$

The desired attitude $\mathbf{Q}_d$, the desired angular velocity ω_d and the desired angular acceleration $\dot{\omega}_d$ are all bounded functions. The desired reference is such that the quaternion errors satisfy the quaternion constraint $\tilde{\mathbf{q}}^T\tilde{\mathbf{q}} = 1 - \tilde{\eta}^2$

Provided that the aircraft desired attitude $\mathbf{Q}_d$ is determined, we defined the attitude tracking error, describing the discrepancy between the vehicle's attitude and its desired attitude,given by

$$\tilde{\mathbf{Q}} = \mathbf{Q}_d^{-1} \otimes \mathbf{Q} \tag{4.38}$$

namely $\tilde{\mathbf{Q}} = \left(\tilde{\mathbf{q}}^T, \tilde{\eta}\right)^T$ with $\tilde{\eta} \in [-1, 1]$ by definition, governed by the unit-quaternion dynamics.

$$\dot{\tilde{\mathbf{q}}} = \frac{1}{2}\left(\tilde{\eta}\mathbf{I}_3 + \mathbf{S}\left(\tilde{\mathbf{q}}\right)\right)\tilde{\omega} \qquad \dot{\tilde{\eta}} = -\frac{1}{2}\mathbf{q}^T\tilde{\omega} \tag{4.39}$$

$$\tilde{\omega} = \omega - \mathbf{R}(\tilde{\mathbf{Q}})\omega_d \tag{4.40}$$

The control goal is to steer $\tilde{\mathbf{q}}(t)$ to zero, with respect to the quaternion constraint, $\tilde{\eta}$ must converge to $+1$ or -1.

where $\tilde{\omega}$ is the angular velocity error vector and $\mathbf{R}(\tilde{\mathbf{Q}})$ is the rotation matrix related to $\tilde{\mathbf{Q}}$, and given by $\mathbf{R}(\tilde{\mathbf{Q}}) = \mathbf{R}(\mathbf{Q})\mathbf{R}(\mathbf{Q}_d)^T$

we can see that the attitude tracking is achieve when $\mathbf{Q}$ coincides with $\mathbf{Q}_d$ due redundancy of the quaternion coordinate has two equlibria, which represent by $\tilde{\mathbf{Q}} = (\mathbf{0}_3^T, \pm 1)^T$ and $\tilde{\omega} = \mathbf{0}_3$ with $\mathbf{0}_3$ =col[0, 0, 0].

For the purpose of analysis we translate the problem of stabilizing an equilibrium to that of stabilizing the origin. For this reason the attitude error vector is defined $\tilde{\mathbf{Q}}_\pm = [\mathbf{q}^T, 1 \pm \tilde{\eta}]^T$. The kinematic related to the attitude error can be expressed as

$$\dot{\tilde{\mathbf{Q}}}_\pm = \frac{1}{2}\mathbf{T}(\tilde{\mathbf{Q}}_\pm)\tilde{\omega} \tag{4.41}$$

where

$$\mathbf{T}(\tilde{\mathbf{Q}}_\pm) = \begin{bmatrix} \tilde{\eta}\mathbf{I}_3 + \mathbf{S}(\tilde{\mathbf{q}}) \\ \pm\tilde{\mathbf{q}}^T \end{bmatrix}$$

4.2.5 Backstepping Control

To solve the problem of designing a globally asymptotically stabilizing control law for the identity element of $SO(3)$, the rigid body dynamics 2.42 is presented by two subsystem, taking the first one with the force as the control input and considering the rotational dynamics 5.36 with unit quaternion representation choosing ω as the virtual control, and $\mathbf{Q}_d$ desired attitude to be known and design a control input such that the error attitude $\tilde{\mathbf{q}}$ converge asymptotically to zero, and the attitude quaternion follows the desired attitude.

Position Control: Based on the rotational dynamics 5.36 with unit quaternion.

$$\dot{P} = R(Q)V \tag{4.42}$$

with $R(Q) = \mathbf{I}_3 + 2\eta\mathbf{S}(\mathbf{q}) + 2\mathbf{S}(\mathbf{q})^2$, and for a unit-quaternion, we have $\mathbf{q} = [0 \quad 0 \quad 0]^T$

$$\dot{P} = \mathbf{I}_3 V \tag{4.43}$$

where $\mathbf{I}_3$ is the identity matrix, we obtain

$$\dot{P} = V \tag{4.44}$$

Now for the position control let V be the virtual input for 5.44, which brings the subsystem to the stability. The goal of this control is to make the position of the vehicle converge to the desired position, and the desired continuous signal $P_d(t)$ and $\dot{P}_d(t)$ are given. For this it is necessary to define a signal $V_d t$ that brings the $P(t)$ to the

desired position $P_d(t)$, therefore the positions tracking error dynamics are represented as:

$$\dot{\tilde{P}} = \dot{P} - \dot{P}_d \tag{4.45}$$

with the position and velocity tracking error $\tilde{P} = P - P_d$, $\tilde{V} = V - V_d$

Let the Lyapunov Function Candidate (LFC) be

$$W_1 = \frac{1}{2}\tilde{P}^T\tilde{P} \tag{4.46}$$

The time derivative of w_1 along the solution of position error

$$\dot{W}_1 = \frac{1}{2}\tilde{P}^T(\tilde{V} + V_d - \dot{P}_d) \tag{4.47}$$

with $V = \tilde{V} + V_d$ and $V_d = -K_p\tilde{P} + \dot{P}_d$

$$\dot{W}_1 = -\tilde{P}^T K_p\tilde{P} + \tilde{P}^T\tilde{V} \tag{4.48}$$

Velocity Control: Now in the first subsystem, the dynamics acceleration is considered, by considering that the Coriolis acceleration is also significant in high-speed flight; it is zero for an aircraft flying due North or South at the equator and reaches its maximum value at the poles or for flight due East or West at any latitude. Its significance can be estimated by equating its value to the centripetal acceleration, in low, constant-altitude flight, at 45 deg latitude [55], to achieve the goal of the control and for our benefit we considered that the Coriolis acceleration is zero. In this fact the acceleration of the

system is rewritten as

$$\dot{V} = g\hat{e} - \frac{F}{m} RQ^T \hat{e} \tag{4.49}$$

where m and g are the aircraft mass and the gravitational acceleration, $\hat{e} = [0 \quad 0 \quad]^T$ is the basis vector.

Representing the acceleration dynamics in function of error we have

$$\dot{\tilde{V}} = g\hat{e} - \frac{F}{m} RQ^T \hat{e} - \dot{V}_d \tag{4.50}$$

$\frac{F}{m} RQ^T \hat{e} = \sigma$ where $\tilde{\sigma} = \sigma - \sigma_d$

$$\dot{\tilde{V}} = g\hat{e} - (\tilde{\sigma} + \sigma_d) - \dot{V}_d \tag{4.51}$$

for the extraction force, we used the process as in [61]. Now let the Lyapunov Function Candidate be

$$W_2 = W_1 + \frac{1}{2} \tilde{V}^T \tilde{V} \tag{4.52}$$

The time derivative of W_2 is represented as follow

$$\dot{W}_2 = \dot{W}_1 + \frac{1}{2} \tilde{V}^T (g\hat{e} - (\tilde{\sigma} + \sigma_d) - \dot{V}_d) \tag{4.53}$$

Taking $\sigma_d = K_v \tilde{V} + g\hat{e} + \tilde{P} - \dot{V}_d$, that yields

$$\dot{W}_2 = -\tilde{P}^T K_p \tilde{P} - \tilde{V}^T K_v \tilde{V} - \tilde{V}^T \tilde{\sigma} \tag{4.54}$$

Attitude Control: Regarding the attitude error dynamics, for our purpose the angular velocity error has defined as presented:

$$\tilde{\omega} = \begin{cases} \omega - \mathbf{R}(\tilde{\mathbf{Q}})\omega_d & \textit{if there exist any rotation} \\ \omega - \omega_r & \textit{perfect set point} \end{cases} \tag{4.55a}$$

Considering the error quaternion constraint, Lyapunov Function Candidate (LFC) is chosen as

$$W_3 = (1 - \text{sgn}(\tilde{\eta})\tilde{\eta})^2 + \tilde{q}^T\tilde{q} = 2(1 - \text{sgn}(\tilde{\eta})\tilde{\eta}) \tag{4.56}$$

for more simplicity $\tilde{S} = \text{sgn}(\tilde{\eta})$ and the signum function is used to define a nonzero as

$$\text{sgn}(\tilde{\eta}) = \begin{cases} -1 & \tilde{\eta} < 0 \\ 1 & \tilde{\eta} \geq 0 \end{cases} \tag{4.57}$$

is a hybrid variable used in [62] to avoid the singularity when $\tilde{\eta} = 0$, rewritten the LFC as follow

$$W_3 = 2(1 - \tilde{S}\tilde{\eta}) \tag{4.58}$$

The time derivative of W_3

$$\dot{W}_3 = -2\tilde{S}\dot{\tilde{\eta}} \tag{4.59}$$

Substituting the $\dot{\tilde{\eta}}$, we have

$$\dot{W}_3 = \tilde{S}\tilde{\mathbf{q}}^T\tilde{\omega} \tag{4.60}$$

Substituting the $\tilde{\omega}$, we get

$$\dot{W}_3 = \tilde{S}\tilde{\mathbf{q}}^T(\omega - \mathbf{R}(\tilde{\mathbf{Q}})\omega_d) \tag{4.61}$$

In a perfect set point the angular velocity can be shown as $\omega = \tilde{\omega} - \omega_r$, in view of that analysis the time derivative of W_w can change into

$$\dot{W}_3 = \tilde{S}\tilde{\mathbf{q}}^T(\tilde{\omega} + \omega_r - \mathbf{R}(\tilde{\mathbf{Q}})\omega_d) \tag{4.62}$$

with $\tilde{\sigma} = \Gamma\tilde{\mathbf{q}}$ and $\vartheta = \frac{F_c}{m}$ we have

$$\tilde{\sigma} = \vartheta R(\mathbf{q})\hat{e} - \sigma_d \tag{4.63}$$

$$\tilde{\sigma} = \vartheta\left(R(\mathbf{q}) - R(\mathbf{q}_d)\right)\hat{e} \tag{4.64}$$

using the fact that $R(\mathbf{q}) = R(\tilde{\mathbf{q}})R(\mathbf{q}_d)$

$$\tilde{\sigma} = \vartheta\left(R(\tilde{\mathbf{q}})R(\mathbf{q}_d) - R(\mathbf{q}_d)\right)\hat{e} \tag{4.65}$$

$$\tilde{\sigma} = \vartheta \left(R(\tilde{\mathbf{q}}) - \mathbf{I}_3 \right) R(\mathbf{q}_d)\hat{e} \tag{4.66}$$

$$\tilde{\sigma} = 2\vartheta \left(-\tilde{\eta}\mathbf{S}(\tilde{\mathbf{q}}) + \mathbf{S}^2(\tilde{\mathbf{q}}) \right) R(\mathbf{q}_d)\hat{e} \tag{4.67}$$

$$\tilde{\sigma} = 2\vartheta \left(\tilde{\eta}\mathbf{I}_3 - \mathbf{S}(\tilde{\mathbf{q}}) \right) \mathbf{S}(R(\mathbf{q}_d)\hat{e})\tilde{\mathbf{q}} \tag{4.68}$$

such that $\Gamma(\tilde{\mathbf{q}}, \mathbf{q}_d, F_c) = 2\vartheta \left(\tilde{\eta}\mathbf{I}_3 - \mathbf{S}(\tilde{\mathbf{q}}) \right) \mathbf{S}(R(\mathbf{q}_d)\hat{e})$

$$\tilde{\sigma} = \Gamma(\tilde{\mathbf{q}}, \mathbf{q}_d, F_c)\tilde{\mathbf{q}} \tag{4.69}$$

with ω_r as virtual control, that brings the system to stability, therefore it defined as

$$\omega_r = -\tilde{S}\mathbf{K}_q\tilde{q} + \mathbf{R}(\tilde{\mathbf{Q}})\omega_d + \Gamma^T\tilde{\mathbf{q}} \tag{4.70}$$

$\dot{W}_3$ becomes

$$\dot{W}_3 = -\tilde{P}^T K_p \tilde{P} - \tilde{V}^T K_v \tilde{V} - \tilde{\mathbf{q}}^T K_q \tilde{\mathbf{q}} + \tilde{S}\tilde{\mathbf{q}}^T\tilde{\omega} \tag{4.71}$$

with $\tilde{S}^2 = 1$

Angular Velocity Control: The idea is to a τ that make the actual angular velocity ω reaches the reference angular velocity ω_r, taking the subsystem 5.36b we get

$$\mathbf{J}(\dot{\tilde{\omega}} + \dot{\omega}_r) = \tau - \mathbf{s}(\tilde{\omega} + \omega_r)\mathbf{J}(\tilde{\omega} + \omega_r) \tag{4.72}$$

Using the cross product properties ($b \times a = -a \times b$), we have

$$\mathbf{J}\dot{\tilde{\omega}} = \tau + \mathbf{J}(\tilde{\omega} \times (\tilde{\omega} + \omega_r) + \omega_r) - \mathbf{J}\dot{\omega}_r \tag{4.73}$$

$$\mathbf{J}\dot{\tilde{\omega}} = \tau + \mathbf{J}\tilde{\omega}(\tilde{\omega} + \omega_r) + \mathbf{s}(\mathbf{J}\omega_r)(\tilde{\omega} + \omega_r) - \mathbf{J}\dot{\omega}_r \tag{4.74}$$

$$\mathbf{J}\dot{\tilde{\omega}} = \tau + \mathbf{s}(\mathbf{J}\tilde{\omega})(\tilde{\omega} + \omega_r) + \mathbf{s}(\mathbf{J}\omega_r)(\tilde{\omega} + \omega_r) - \mathbf{J}\dot{\omega}_r \tag{4.75}$$

For more simplicity $\mathbf{J}\dot{\tilde{\omega}}$ is changed into

$$\mathbf{J}\dot{\tilde{\omega}} = \tau + \Sigma(\tilde{\omega}, \omega_r)\tilde{\omega} + \phi(\omega_r, \dot{\tilde{\omega}}_r) - \mathbf{s}(\omega_r)\mathbf{J}\tilde{\omega} \tag{4.76}$$

$$\Sigma(\tilde{\omega}, \omega_r) = \mathbf{s}(\mathbf{J}\tilde{\omega}) + \mathbf{s}(\mathbf{J}\omega_r) \tag{4.77a}$$

$$\phi(\omega_r, \dot{\tilde{\omega}}_r) = \mathbf{s}(\mathbf{J}\omega_r)\omega_r - \mathbf{J}\dot{\omega}_r \tag{4.77b}$$

Taking a second Lyapunov Function Candidate

$$W_4 = W_3 + \frac{1}{2}\tilde{\omega}^T\mathbf{J}\tilde{\omega} \tag{4.78}$$

the time derivative of the second LFC is shown as

$$\dot{W}_4 = \dot{W}_3 + \frac{1}{2}\tilde{\omega}^T\mathbf{J}\dot{\tilde{\omega}} \tag{4.79}$$

therefore we get

$$\dot{W}_4 = \dot{W}_3 + \frac{1}{2}\tilde{\omega}^T(\tau + \Sigma(\tilde{\omega}, \omega_r)\tilde{\omega} + \phi(\omega_r, \dot{\tilde{\omega}}_r) - \mathbf{s}(\omega_r)\mathbf{J}\tilde{\omega}) \tag{4.80}$$

Choosing the control input as

$$\tau = -K_\omega\tilde{\omega} - \tilde{S}\tilde{\mathbf{q}} + \mathbf{s}(\omega_r)\mathbf{J}\tilde{\omega} - \phi(\omega_r, \dot{\tilde{\omega}}_r) \tag{4.81}$$

notice that by the properties of cross product $\tilde{\omega}^T\Sigma(\tilde{\omega}, \omega_r)\tilde{\omega} = 0$, which yields $\dot{W}_4$ to becomes a negative definite function such that

$$\dot{W}_4 = -\tilde{P}^T K_p \tilde{P} - \tilde{V}^T K_v \tilde{V} - \tilde{\mathbf{q}}^T K_q \tilde{\mathbf{q}} - \tilde{\omega}^T K_\omega \tilde{\omega} < 0 \tag{4.82}$$

In this work the procedure and proof of the W_4 switch, in [63] is used.

4.2.6 Transitions Control

To change between hover and level flight modes, it is required to implement the transitional maneuvers, which are broken down into parts, such that one control mode is executed at a time. Stall is avoided, throughout the maneuvers. During the actual transition, only pitch rotations are performed from hover to level flight and vice versa. The methodology was not designed to optimize altitude deviation. Results from actual transitions performed in simulation and hardware are given to validate the methods presented.

Hover-to-Level Flight

Hover-to-level flight transitions are executed in two scenarios. In the first scenario, the aircraft rolls to align its underside with the direction of the desired way-point path by considering that the roll and yaw angle are set to zero. For a such rotation the desired quaternion is performed by the Euler's angle. Since the error between the quaternion and desired quaternion is reached a considerable point, the second scenario is executed. The actual transition occurs, where the desired quaternion converges to the set path, resulting in a pitch forward to level flight rotation. Throughout the entire transition maneuver, throttle is set full to increase airspeed and avoid stall conditions.

Level-to-Hover Flight

Level-to-hover flight transitions are performed in the same way. As the vehicle is reaching to a hover way-point, the normal level flight controller is employed. When the distance to the desired point is reduced below a predetermined value, the transition is initiated. In the first scenario, the aircraft is pitched up to a vertical orientation, such that the underside points in the direction of the heading that was measured before the rotation was executed (by the another function such as illustrated in the following equation) [64]. Once this is accomplished, the second scenario begins wherein the vehicle rotates to the vertical quaternion and finally, the normal hover position controller is implemented. Throughout this maneuver, throttle is set from the altitude hover control method. Because the approach speed of the aircraft is relatively large and the pull-up maneuver is executed quickly, aircraft stall is not of significant concern.

$$\begin{bmatrix} \phi \\ \theta \\ \psi \end{bmatrix} = \begin{bmatrix} 0 \\ \frac{\pi}{2} - e^{-t} \\ 0 \end{bmatrix} \tag{4.83}$$

$$\begin{bmatrix} \phi \\ \theta \\ \psi \end{bmatrix} = \begin{bmatrix} 0 \\ \frac{\pi}{2} - \tan^{-1}(t) \\ 0 \end{bmatrix} \tag{4.84}$$

Now the desired quatenion is performed by the Euler's angle reference given.

$$Q_d = \begin{bmatrix} \cos(\phi/2) * \cos(\theta/2) * \cos(\psi/2) + \sin(\phi/2) * \sin(\theta/2) * \sin(\psi/2) \\ \sin(\phi/2) * \cos(\theta/2) * \cos(\psi/2) - \cos(\phi/2) * \sin(\theta/2) * \sin(\psi/2) \\ \cos(\phi/2) * \sin(\theta/2) * \cos(\psi/2) + \sin(\phi/2) * \cos(\theta/2) * \sin(\psi/2) \\ \cos(\phi/2) * \cos(\theta/2) * \sin(\psi/2) - \sin(\phi/2) * \sin(\theta/2) * \cos(\psi/2) \end{bmatrix} \tag{4.85}$$

Note that, for the hover flight mode and transition mode two desired quaternions have implemented, the first one is executed when the vehicle is in the hover flight mode while the second one takes part when the vehicle is switching to level flight and the same desired quaternions are also used in level to hover mode by taking the inverse of the second one.

Chapter 5

Simulations

5.1 Longitudinal Simulations

To illustrate the behavior of the proposed flight path angle control laws, implemented through the backstepping control laws, the control system contains a control allocator, distributing the desired aerodynamic moment to the control surfaces. For flight path angle γ control, integral control is also included to achieve set-point regulation despite model errors.

we illustrate through simulation results of the controllers developed for a Quad Rotor Tail-Sitter UAV. The system's equations of motion of the aircraft longitudinal dynamic by equations 5.1c -5.1d, with a constant parameter of thrust and numerical coefficients C_L , C_D are obtained. The physical parameters are: $\rho = 1.2Kg/m^3$ which supposed to be calculated online, as the density of wind is depend on the temperature and other factors, but in this work we use a constant value for a realistic simulation, $m = 3kg$ is the mass of the vehicle, and for our purpose we used a constant thrust $F_T = 15N$, to $150N$.

Fig. , shows the time evolution of the flight path angle γ response compared to its reference linear response also shows time evolution of the angle of attack α response.

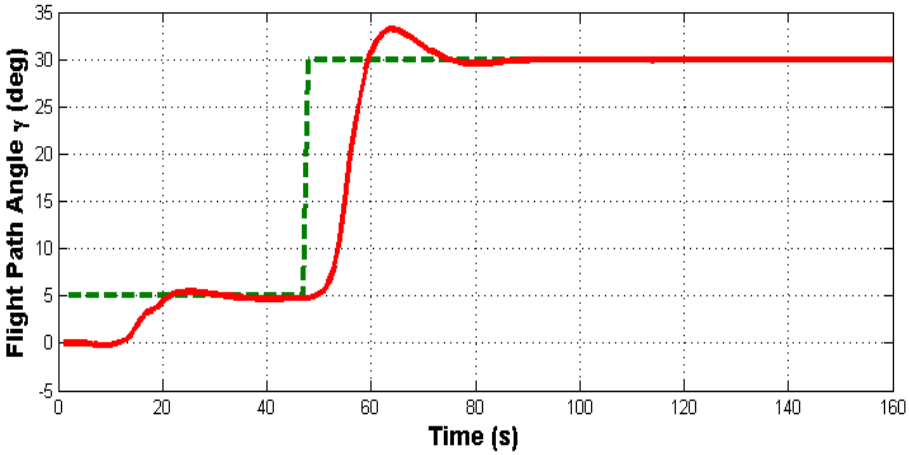

(a) Flight Path Angle

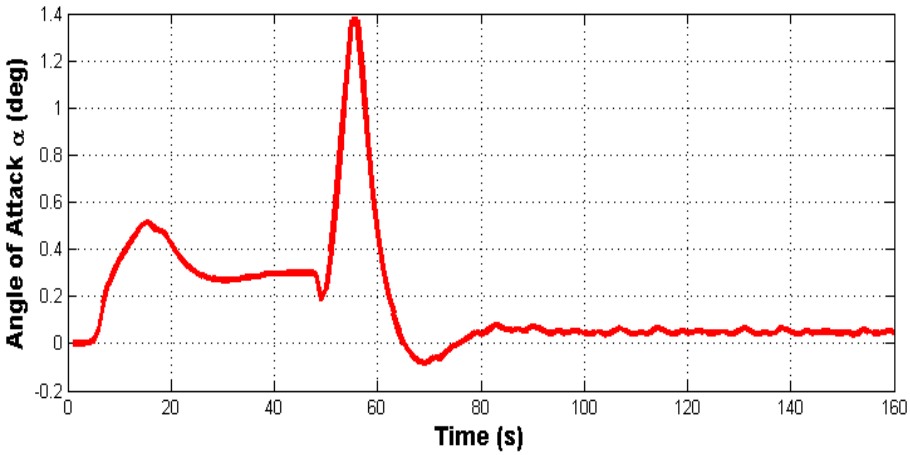

(b) Angle of Attack

Fig. 5.1: Path and Attack

Figure 6.2, shows the control signal, aileron deflection δ_e and the time evolution of pitch acceleration $\dot{q}$.

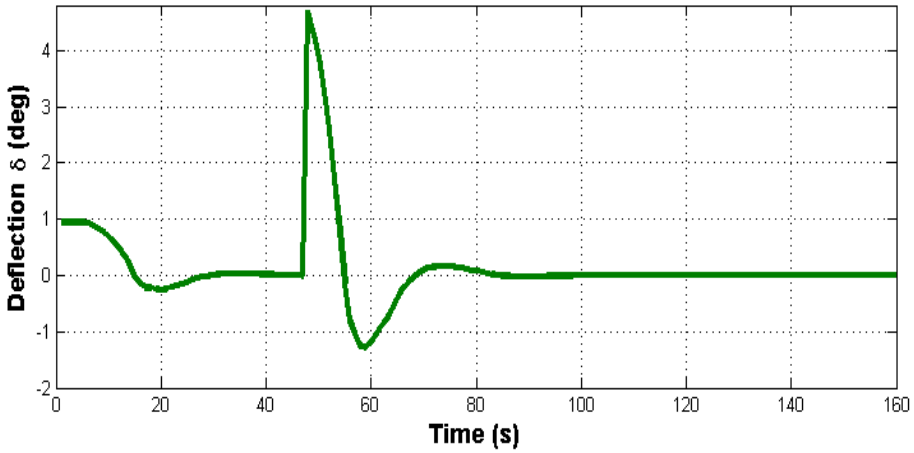

(a) Aileron Deflection

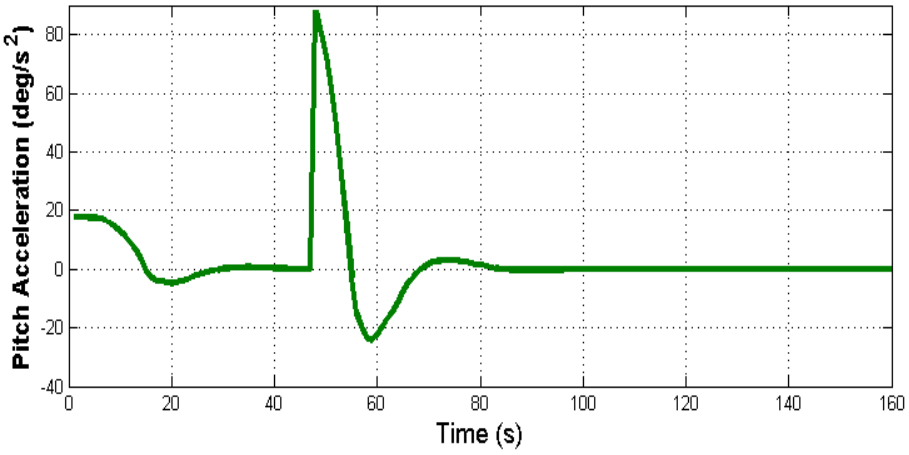

(b) Angular Pitch Acceleration

Fig. 5.2: Aileron Deflection and Angular Pitch Acceleration

Figure 6.3, shows the time evolution of pitch rate $\dot{\theta}$ and the pitch angles $\dot{q}$.

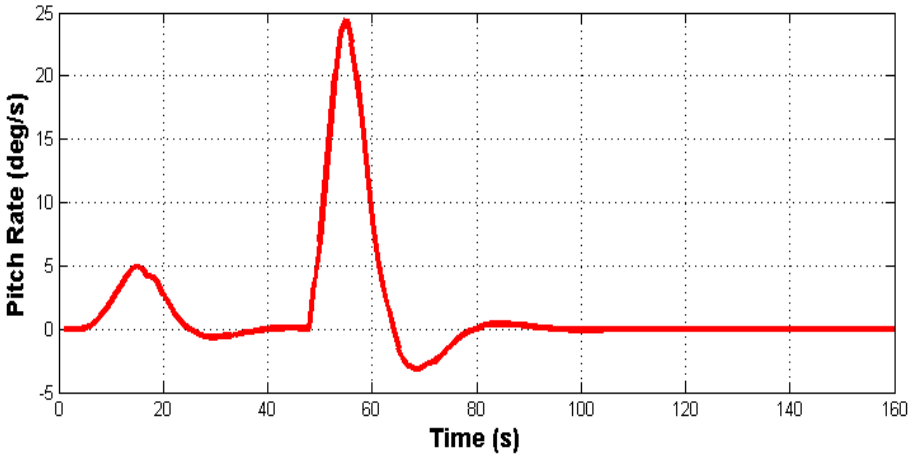

(a) Pitch Rate of Longitudinal Dynamic

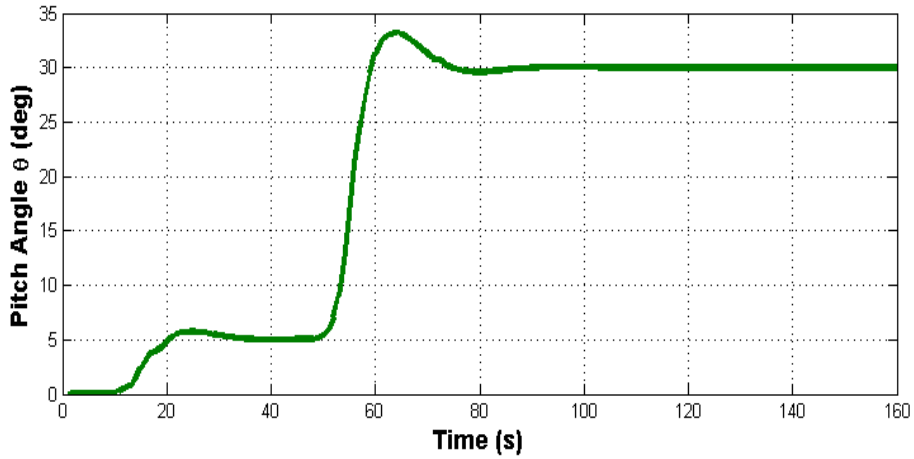

(b) Pitch Angle of Longitudinal Dynamic

Fig. 5.3: Pitch Rate and Pitch Angle

5.2 Quaternion Based Trajectory Tracking

All simulations have been carried out on the nonlinear vehicle model presented in [59], with the back-stepping controller are presented to illustrate the effectiveness of the proposed control scheme. The aircraft model has considered as a rigid body of mass $m = 3.5kg$, with inertial matrix $J = diag(col(0.13, 0.10, 0.04))kgm^2$. The simulation parameters has presented in the following table.

Simulation parameters	
P(0)	$(2, -6, 9)$
V(0)	$(0, 0, 0)$
Q(0)	$(0, 0, 0, 1)$
$\omega(0)$	$(0, 0, 0)$
K_p	0.5
K_v	0.05
g	9.8

Table 5.1: Simulation Prameters

$$V_d = -K_p\tilde{P} + \dot{P}_d$$
$$\sigma_d = K_v\tilde{V} + g\hat{e} + \tilde{P} - \dot{V}_d$$
$$\omega_r = -\tilde{S}\mathbf{K}_q\tilde{q} + \mathbf{R}(\tilde{\mathbf{Q}})\omega_d + \Gamma^T\tilde{\mathbf{q}}$$
$$\tau = -K_\omega\tilde{\omega} - \tilde{S}\tilde{\mathbf{q}} + \mathbf{s}(\omega_r)\mathbf{J}\tilde{\omega} - \phi(\omega_r, \dot{\tilde{\omega}}_r)$$

Table 5.2: Control Signal

Translational Simulations

The desired tracking in this simulation is a position tracking given by $P_d = [cos(0.1t + 2)\, sin(0.1t + 2.4)\, sin(0.1t)cos(0.1t)]^T m$. The following figure plotted the three components of the position and the velocity tracking errors.

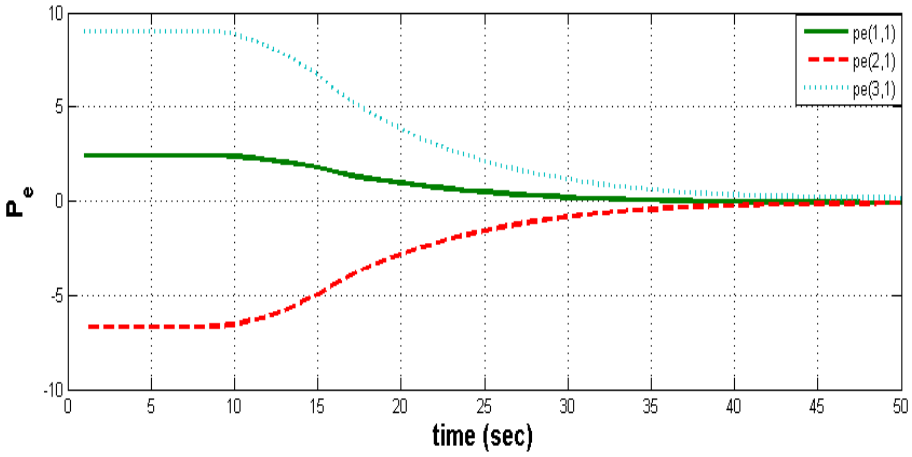

(a) Position Tracking Error

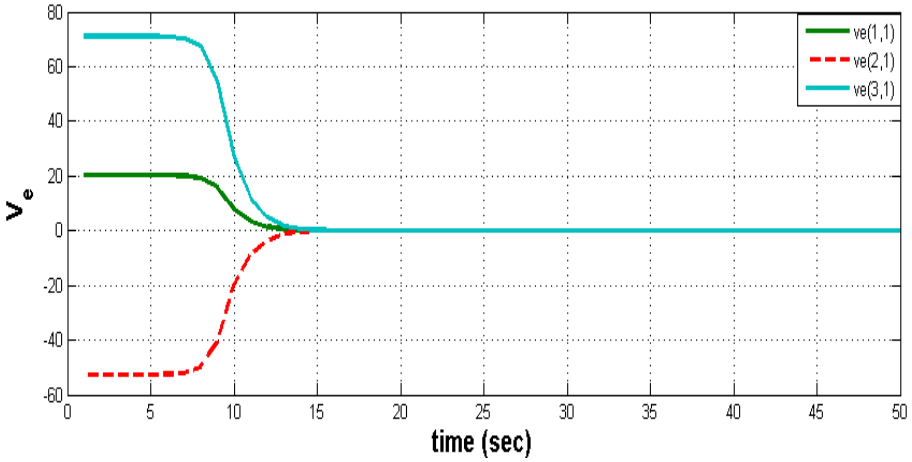

(b) Velocity Tracking Error

Fig. 5.4: Roll and Yaw Transition

Rotational Simulations

In vehicle orientation, attitude determination is very important for two reason, firstly control engineers need to know if the spacecraft attitude is in the right attitude, secondly, it is necessary to know if the spacecraft is not in the perfect position, the attitude information will be compared automatically with the desired attitude, and the error information is then used to calculate how much action is needed for each actuator to bring the spacecraft to the desired attitude. A simulation is presented to study contrasting the proposed hybrid control scheme, where two equilibrium are considered, one of them is chosen a priory, assuming that the controller is hybrid, and a switching technique is introduced to determine the reference equilibrium with the sign of $\tilde{\eta}$ is constant for all t.

Figure 6.5 illustrates the three components of the attitude of the aircraft using the switching technique, where the first plot shows a switching to -1, while the second one illustrates a switching to $+1$. Comparing these two plots, we noticed that there exist a change in the attitude of the vehicle, which means, when the switch is switching to negative o positive value, that causes the components vector of the attitude of the vehicle converge to that value while the scalar part is not affected by sign of the desired value and also illustrates the actual angular velocity of the aircraft.

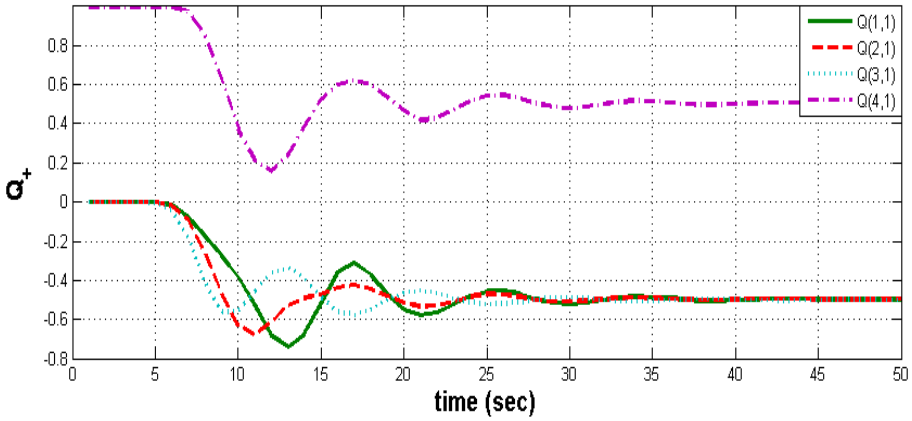

(a) Quaternion Hybrid (plus)

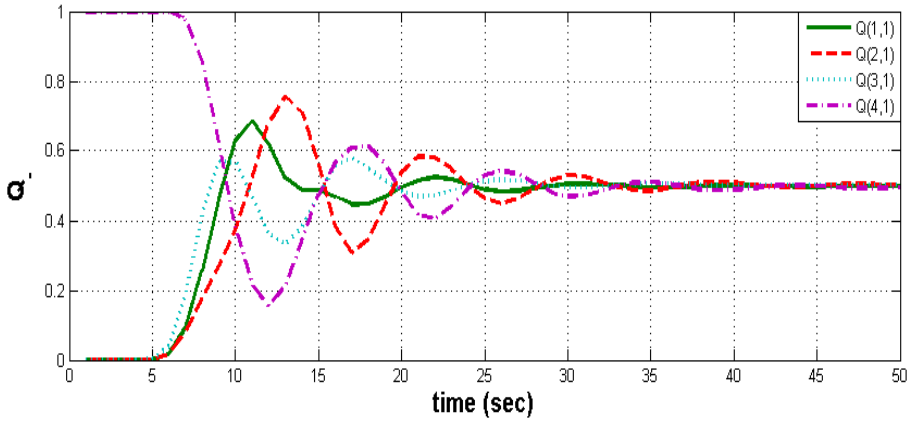

(b) Quaternion Hybrid (minus)

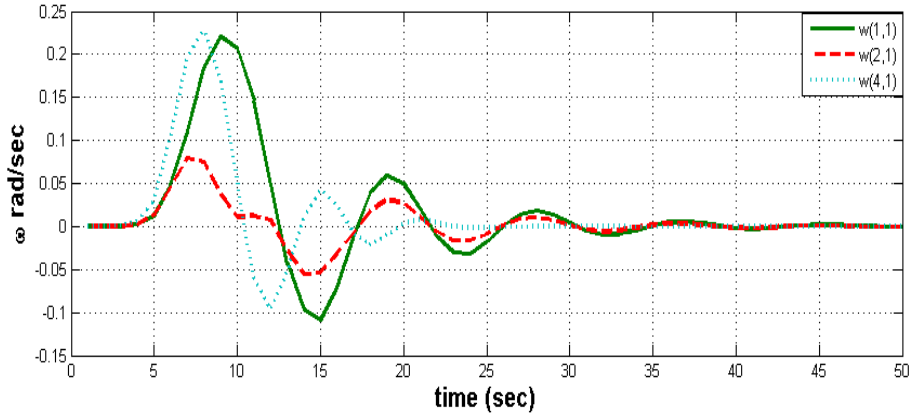

(c) Angular Velocity

Fig. 5.5: Quaternion Error Hybrid (minus)

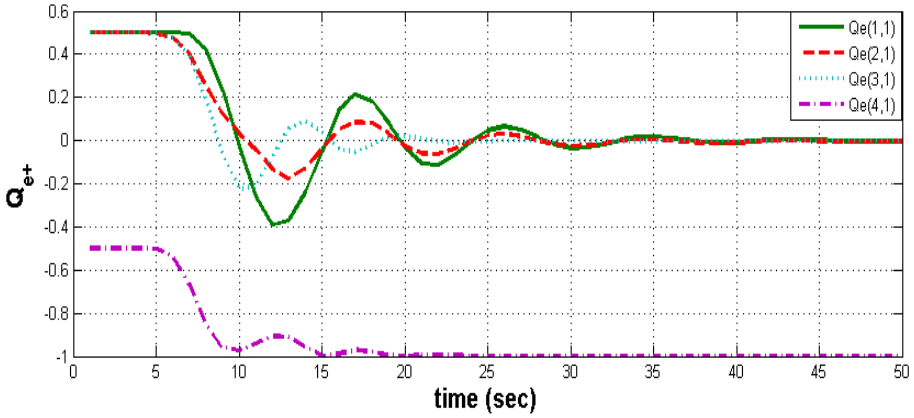

(a) Quaternion Error Hybrid (plus)

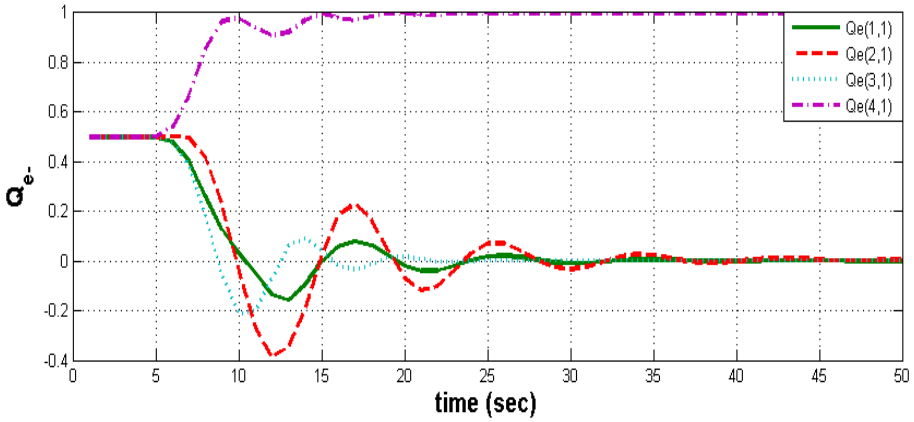

(b) Quaternion Error Hybrid (minus)

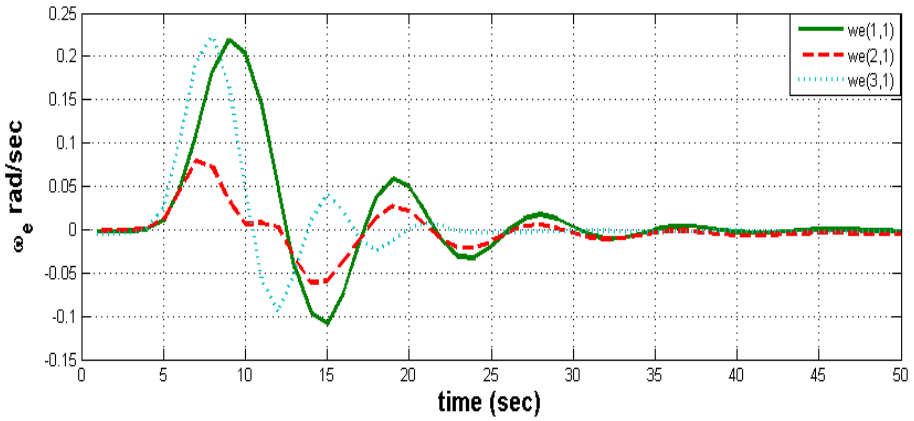

(c) Angular Error Velocity

Fig. 5.6: Quaternion Error Hybrid (minus)

Notice that, these two plots of attitude errors are illustrated clearly the presence of the switching technique, where in the first plot the scalar part is switching to -1 while in the second plot the scalar is switching to $+1$. It is clear that from the actual angular velocity, angular velocity error and component vector of attitude error figure that asymptotic convergence to zero is guaranteed after a few seconds.

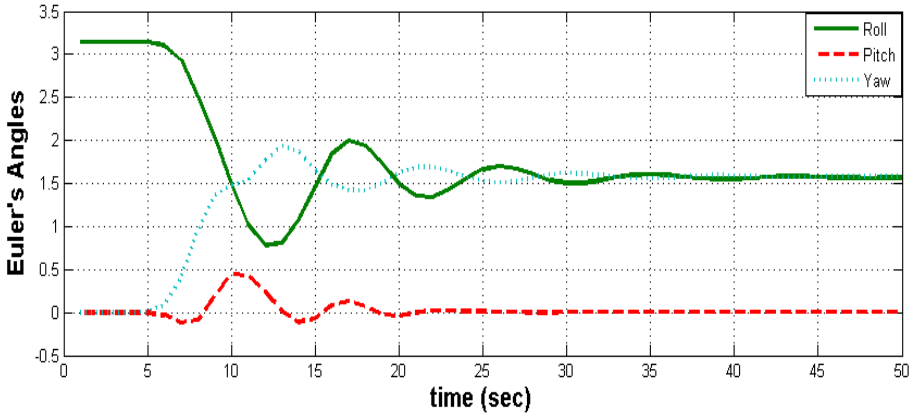

Fig. 5.7: Euler Angles

In the fig. 6.7 we also illustrated a simulation of the Euler angles, which can be compared with the the actual attitude of the aircraft by choosing the desired attitude to be the current attitude. It is important to notice that the roll and yaw angle are converge to a desired value but the pitch angle is converge to zero, which can be interpreted that the aircraft is on the vertical takeoff or landing.

Transition Simulations

Attitude simulation results of the transition methods presented previously are illustrated in Figure 6.8. In Hover-to-level transition, a heading rotation of 90 degrees occurs from 0.5 to 1 seconds. The pitch forward to level flight then can be stated up

from 1.0 second. The level-to-hover flight transition approaches the desired hover point from $\pi/2$, so no heading rotation is required as illustrated in the figure 6.9, only a pitch-up maneuver.

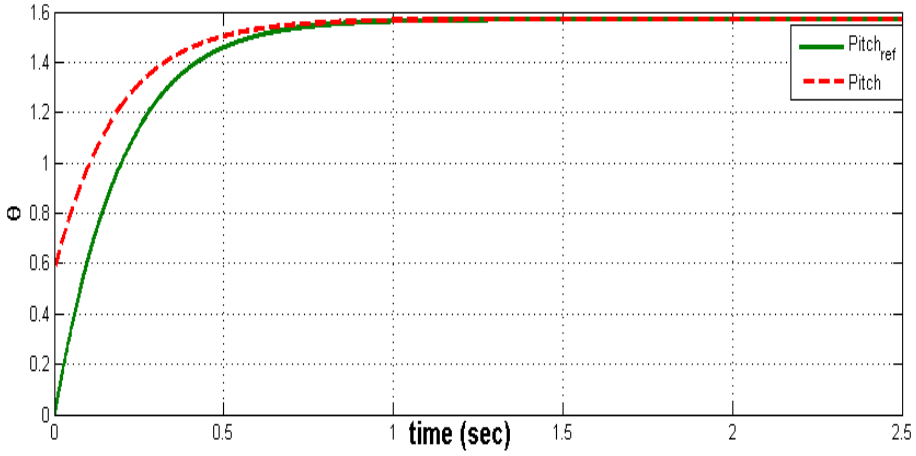

(a) Pitch Transition

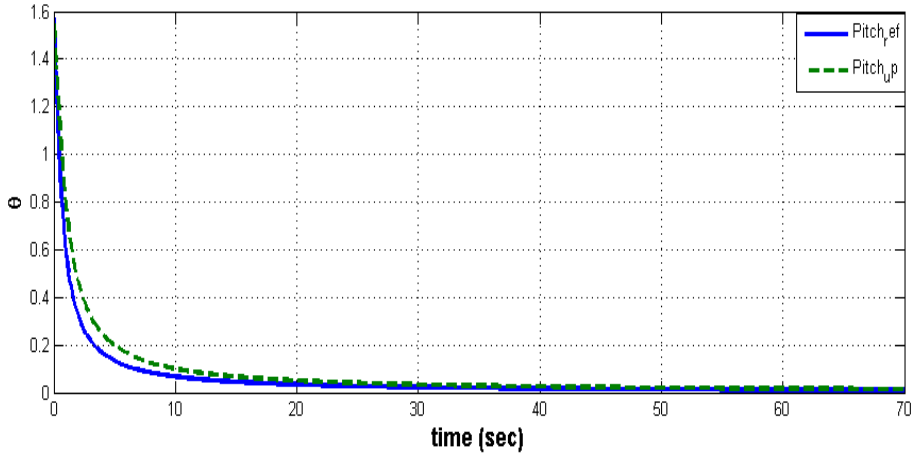

(b) Inverse Pitch Transition

Fig. 5.8: Roll and Yaw Transition

Roll and Yaw are considered to be zero during the maneuver transition, it is clear to see that only pitch is required for this task. Notice that the hover-to-level maneuver is faster than the level-to-hover maneuver since the position of the tail-sitter is more

awkward.

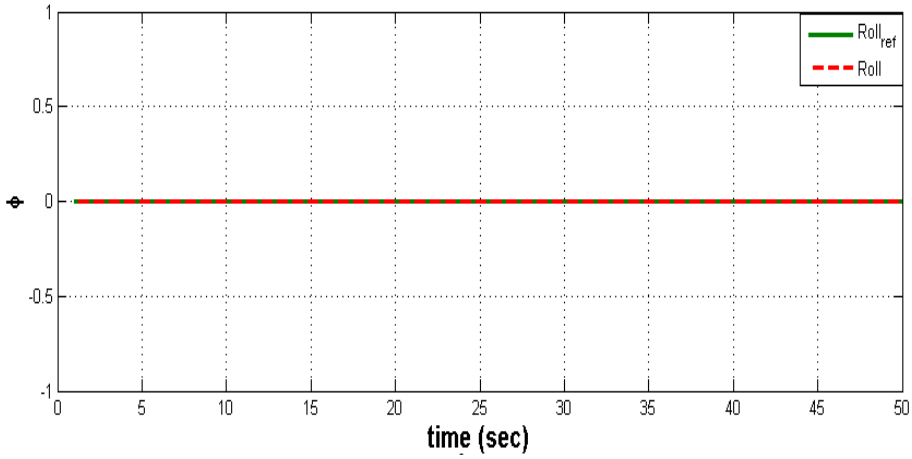

(a) Roll Transition

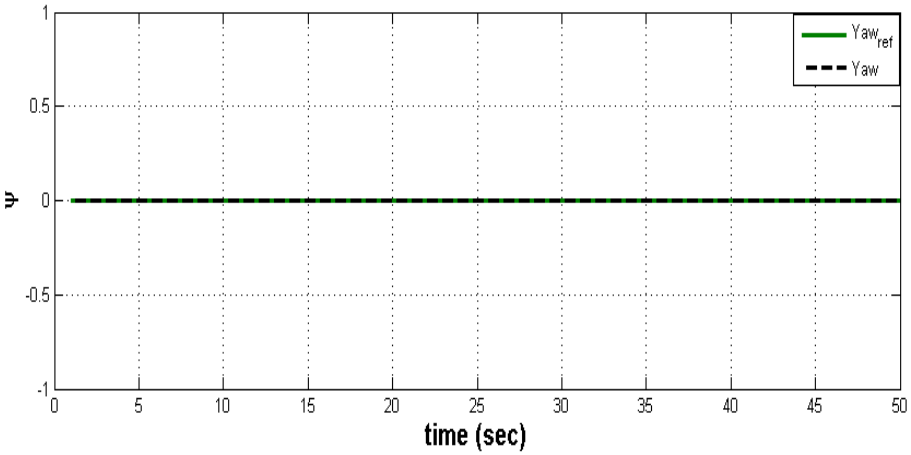

(b) Yaw Transition

Fig. 5.9: Roll and Yaw Transition

5.2.1 Experimental Results

In this section some experimental data from flights performed are shown, which are implemented by a PID control, we have used this type of control because it is easier to handle in the PX4 firmware than backstepping one, since a backstepping technique is

required more information about the vehicle.

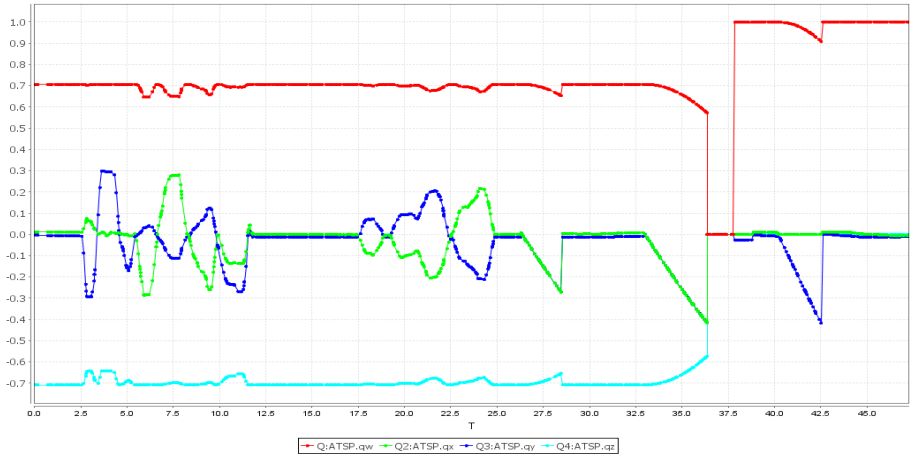

(a) Attitude Quaternion Graphic

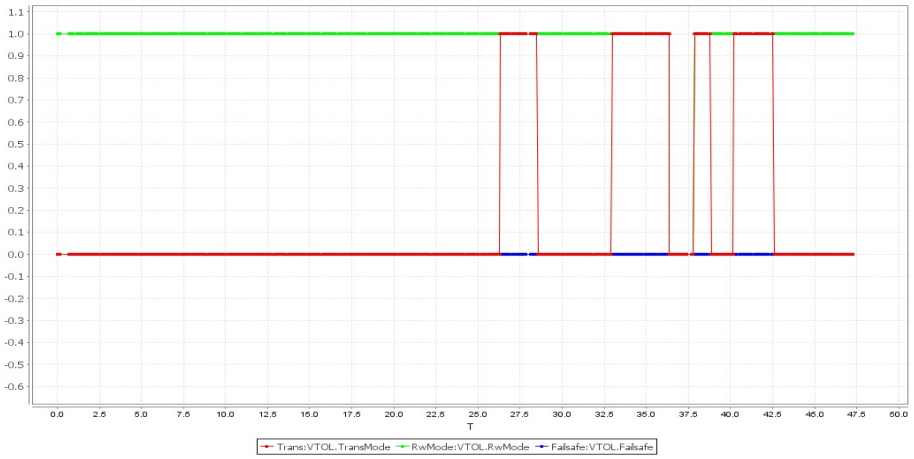

(b) VTOL

Fig. 5.10: Quaternion and Transition mode

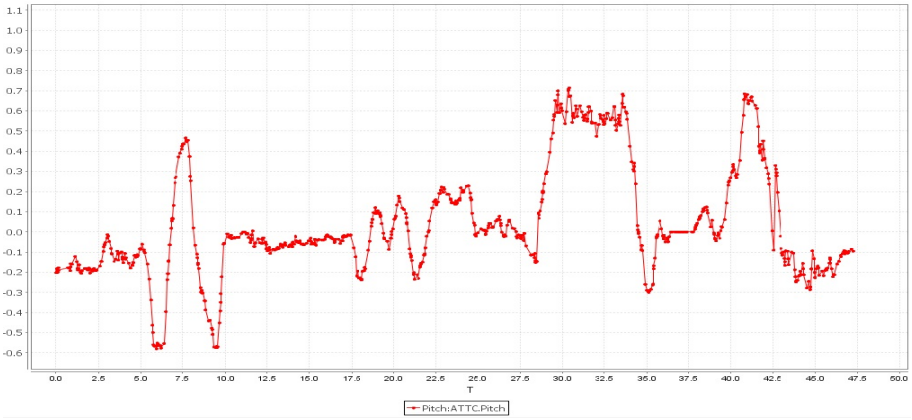

(a) Pitch

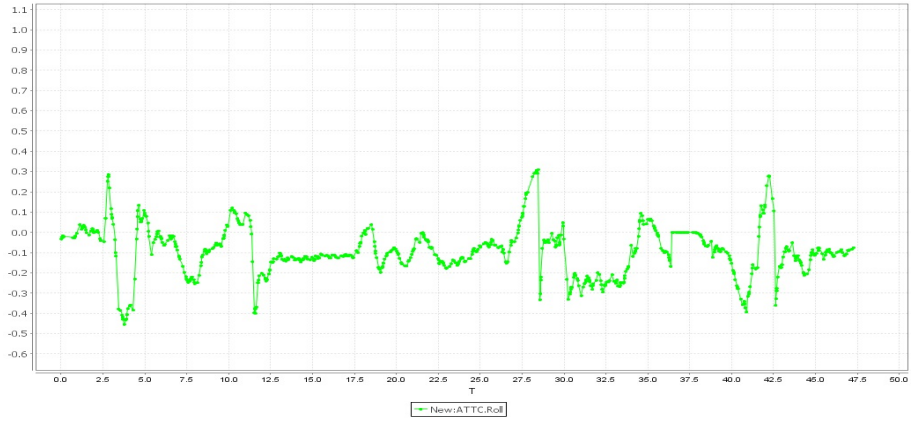

(b) Roll

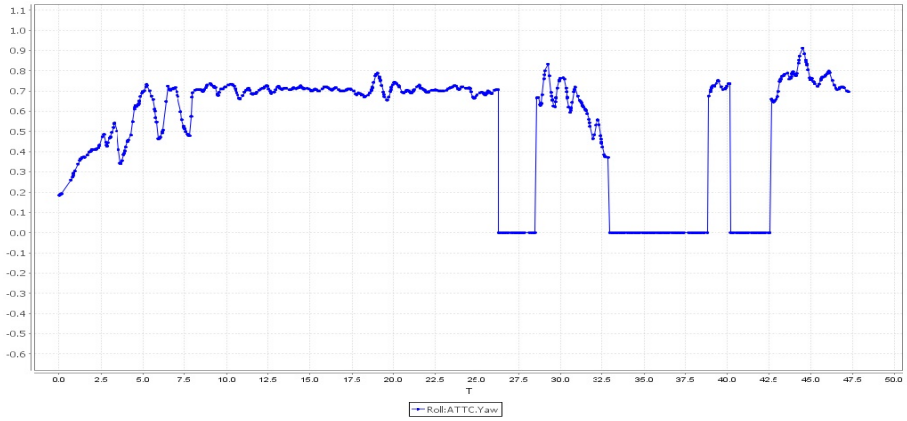

(c) Yaw

Fig. 5.11: Euler's Angles

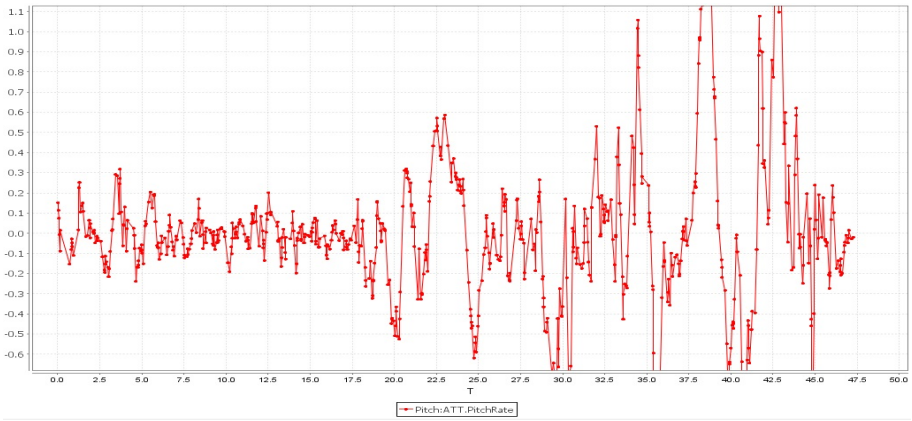

(a) Pitch Rate

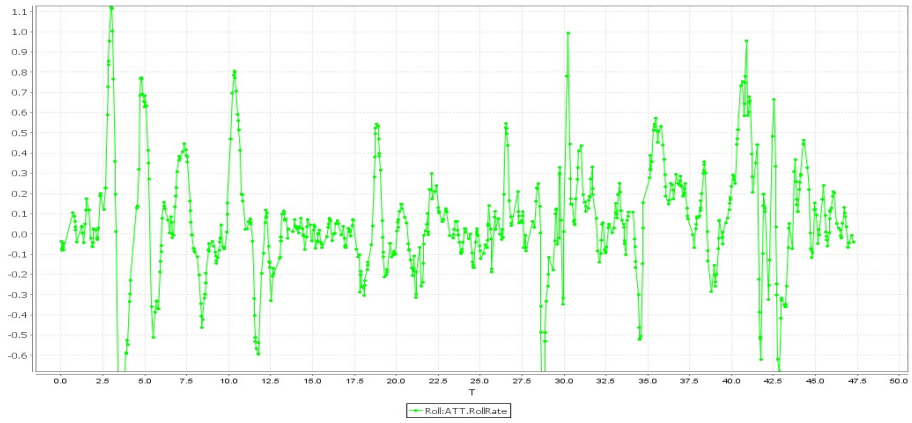

(b) Roll Rate

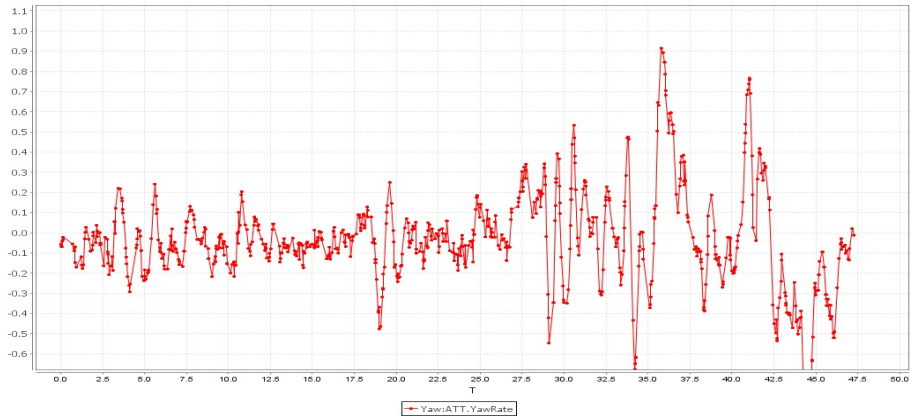

(c) Yaw Rate

Fig. 5.12: Euler Rate

Chapter 6

Design Process

6.1 Introduction

This chapter describes the design process used to develop the air-frame configuration of the tail-sitter UAV, also presented a flight controller with its peripherals and a overview of the tail-sitter manufactured. Which are explained in more detail in the next sections.

6.2 The Design Process

The design process used throughout this project is begun with the establishment of the key design requirements and specifications for the UAV. A design concept was proposed and then scored based on the established specifications. Finally, simulation of flight testing was done to determine whether the design actually fulfilled the specifications.

6.2.1 Prototype Design

The process of design and developing the tail-sitter UAV began with the specification of key design requirements and parameters based on the Quadshot UAV [19]. These requirements and parameters quantify the objective stated in the previous chapters,

which was to design, build, and fly the smallest useful tail-sitter UAV to date. Specifically, the vehicle was designed to be able to achieve the hover-to-level flight transition, level-to-hover flight transition and perform a mission, then return home and land vertically. The concept is studied with detailed of previous tail-sitter aircraft illustrated in table 1.1, specifically in the Quadshot, is a full-scale manned aircraft and smaller UAVs, which was studied to develop a knowledge of previous projects. The tail-sitter was design and a fluid analysis was done, using the SolidWorks and Ansys.

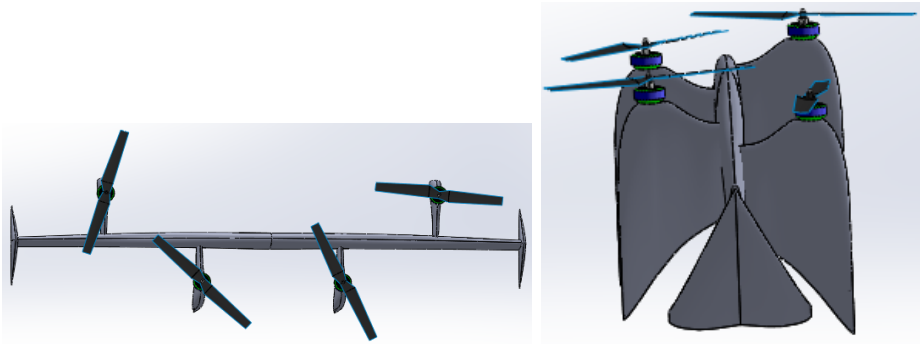

(a) Front View (b) Lateral View

Fig. 6.1: Tail-Sitter.

6.2.2 Manufacturing Analysis

Composites are, by definition, materials consisting of two or more materials which together produce beneficial properties that cannot be attained with any of the constituents alone. One of the most common examples, fiber-reinforced composite materials consist of high strength and high modulus fibers in a matrix material. Reinforced steel bars embedded in concrete provide an example of fiber-reinforced composites [43]. In these composites, the function of the fibers is carrying the load exerted on the composite structure, and providing stiffness, strength, thermal stability and other structural

properties. Matrix material carries out several functions in a composite structure, some which are binding the fibers together and transferring the load to the fibers, and providing protection to reinforcing fibers against chemical attack, mechanical damage and other environmental effects like moisture, humidity, etc [44].Composites have unique advantages over monolithic materials, such as high strength, high stiffness, long fatigue life, low density, and adaptability to the intended function of the structure[45].

They offer further improvements in corrosion resistance, wear resistance, appearance, temperature-dependent behavior, thermal stability, thermal insulation, thermal conductivity, and acoustic insulation. The basis that makes the composites to have superior structural performance stands on their high specific strength (strength to density ratio) and high specific stiffness (modulus to density ratio) and the anisotropic and heterogeneous character of the material.

The anisotropic and heterogeneous character also provides freedom to design a structure with optimum configuration for serving a specific function [46]. The following figure illustrates the mold design, which is divided in two parts, the cavity and the core.

Molding

Building a UAV wing out of composite materials is one of the main part of this work. The composite wing is manufactured using cavity and core molds manually without the vacuum bagging technique. In the following sections of this chapter detailed descriptions of manufacturing process is available. The manufacturing of the cavity and core molds of the wing is explained. Finally, the manufacturing of the wing structure is elucidated in this section.

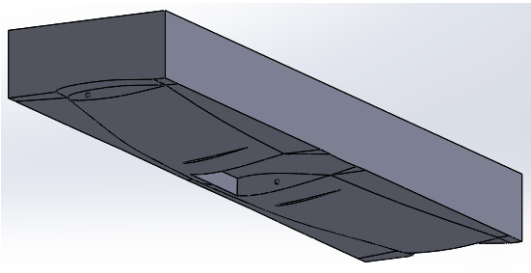

(a) Cavity

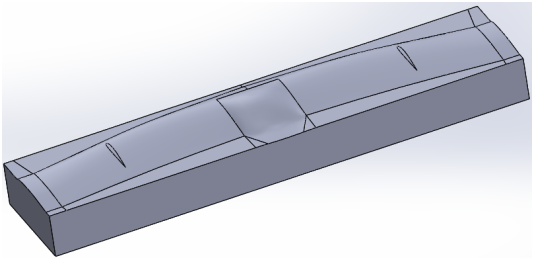

(b) Core

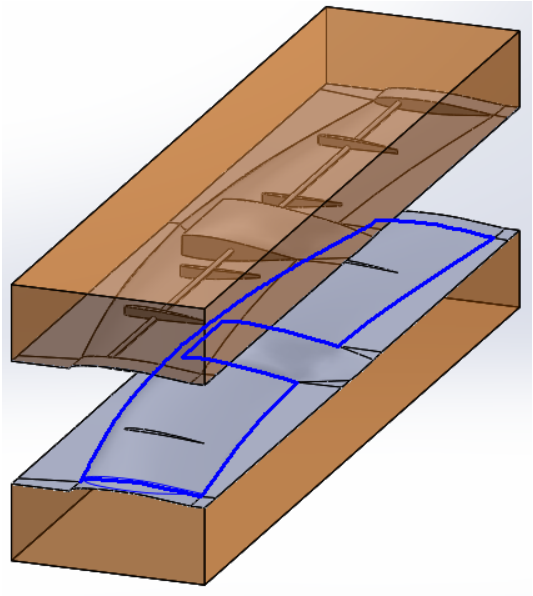

(c) Mold

Fig. 6.2: Mold Design.

As it mentioned previously in this section, a composites materials is a mixing of a variety of materials, also included a kind of chemical material that is applied to the tool surface for preventing the sticking of the laminate to the mold surface. to manufacture the tail-sitter, it is required a process to bring out the mold, for this reason a list of the materials that have been used for this work has shown in the next table.

Table 6.1: List of Materials.

Materials	Quantities
Release Agent 4100	700 g.
Release Film	900 g.
Sponge Application	4 pc.
Tooling Gel Coat	2 kg.
Paintbrushes	8 pc.
Acetone	4 L.
Bast Cloth	1 kg.
Catalyst K-2000	250 g.
Fiberglass Mat	6 kg.
Coremat Xi 3mm or 5mm	6 m^2.
Polyester Resin	6 kg.
Roller Washers $3/4 \times 3$"	2 pc.
Tooling Gel Coat Calibrator	1 pc.
MDF, Triply Wood 55×40 cm	4 pc.
Wood Strips 55×5cm	8 pc.
35×5cm	8 pc.

a) Cutting the wood in the shape of the piece.

b) Stick the piece to the cut wood and Fill up the edge of the piece with clay, stick to the wood base.

c) Clean up the wood and the piece with the bast cloth.

d) With the bast cloth, apply the release agent 4100 over the surface about 3 times.

e) With the Paintbrushes, apply the release film over the surface about 3 times.

f) Now, apply the tooling gel coat over the surface about 3 times. (to determine the thickness of the tooling gel coat the following formula is used $((55\times40)\times0.11)/2 = 110\,g$)(Catalyst K-2000 also used in this process, it depends on how fast do you want the tooling gel coat dries.)

g) For our purpose we used $500\,g$ of Polyester Resin, we also used the catalyst K-2000 to this process for a fast dry. (The same process has used to mold the wing of the tail-sitter)

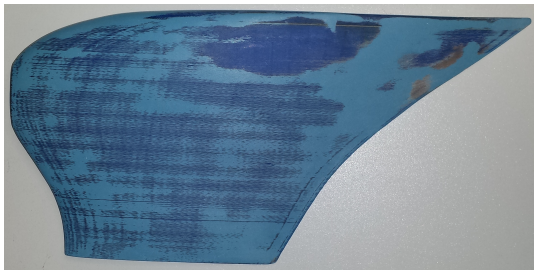

(a) Pylon

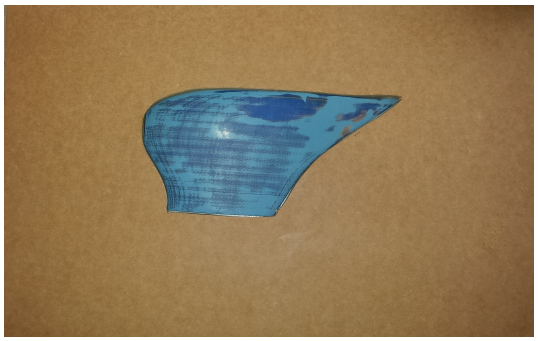

(b) Pylon stocked to the wood

(c) Pylon with Tooling Gel Coat

(d) Applying the Fiber glass

Fig. 6.3: Mold

(a) Front View

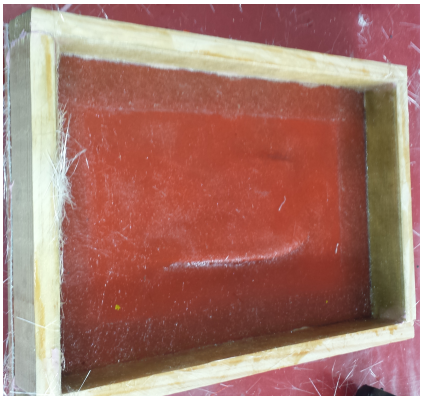

(b) Back View

(c) Complete Mold

(d) Wing

Fig. 6.4: Fiberglass Mold

6.3 Flight Controller Selection

To choose a flight controller for flying an aircraft, it depends on what firmware that is going to be used, and it is also very important to know what will be the application, for our mission we have used the PX4, which fits better on the pixhawk flight controller. First it is important to say there exist three architectures of the pixhawk flight controller. The first architecture created was named Pixhawk v1 which had a two components PX4FMU+PX4IO. There was a second architecture created named Pixhawk v2, this architecture combines the PX4FMU and PX4IO in one hardware controller, in this work this architecture are used to development the application of the tail-sitter, as shown in the following figure. Just recently a third generation of architecture was released, referred as FMUv4 and PixRacer is the first board with this architecture, this architecture is in making. This section provides high level information about how to power Pixhawk and connect its most important peripherals.

6.3.1 Specifications

Processor

- 32bit STM32F427 Cortex M4 core with FPU
- 168 MHz
- 256 KB RAM
- 2 MB Flash
- 32 bit STM32F103 failsafe co-processor

Sensors

- ST Micro L3GD20H 16 bit gyroscope
- ST Micro LSM303D 14 bit accelerometer / magnetometer
- Invensense MPU 6000 3-axis accelerometer/gyroscope
- MEAS MS5611 baromete

Interfaces

- 5x UART (serial ports), one high-power capable, 2x with HW flow control
- 2x CAN (one with internal 3.3V transceiver, one on expansion connector)
- Spektrum DSM / DSM2 / DSM-X Satellite compatible input
- Futaba S.BUS compatible input and output
- PPM sum signal input
- RSSI (PWM or voltage) input
- I2C
- SPI
- 3.3 and 6.6V ADC inputs
- Internal microUSB port and external microUSB port extension

Power System and Protection

- Ideal diode controller with automatic failover
- Servo rail high-power (max. 10V) and high-current (10A+) ready
- All peripheral outputs over-current protected, all inputs ESD protected

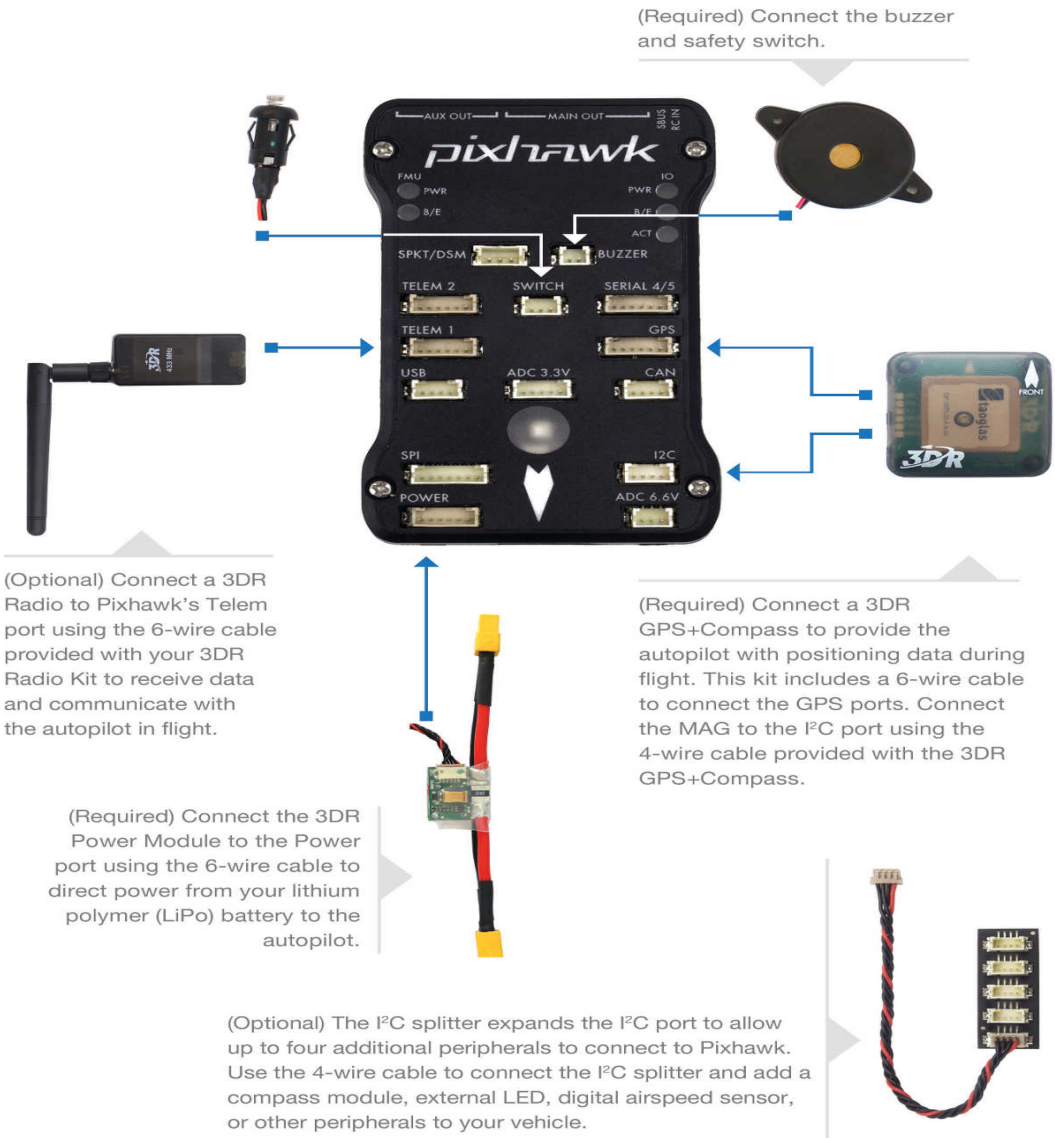

Fig. 6.5: Pixhawk connection

Airspeed Sensor

It features a Measurement Specialties 4525DO sensor, with 1 psi measurement range (roughly up to 100 m/s or 360 km/h or 223 mp/h). Its resolution of 0.84 Pa is quite good, and delivered as 14 bit data from a 24 bit delta-sigma ADC. It also measures temperature to allow to calculate true airspeed from indicated airspeed using the MS5611 static pressure sensor on Pixhawk. As the temperature is not influenced by the heat of nearby processing components, it is much closer to the air temperature than with the previous analog sensor setup. It comes with M3 / 6-32 mounting holes. It is supported on all PX4 autopilot generation boards [47], [48].

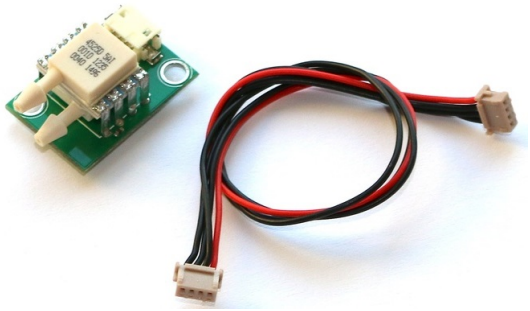

(a) PX4 Airspeed

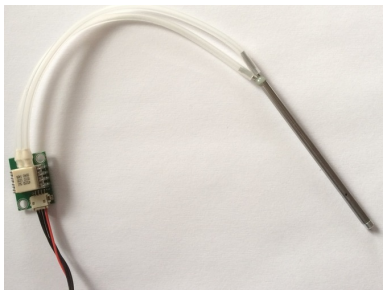

(b) Pitot Tube (Airspeed)

Fig. 6.6: Tail-Sitter.

Remote Control Input

Pixhawk is compatible with PPM remote control (RC) receivers, Futaba S.Bus receivers, and Spektrum DSM,DSM2, and DSM-X Satellite receivers. For traditional single-wire-per-channel (PWM) receivers a PPM encoder can be used to convert the receiver outputs to PPM-SUM. Information about compatible receivers and how they are connected can be found in Compatible RC Transmitter and Receiver Systems (Pix-

hawk/PX4).

Fig. 6.7: DX8 Spektrum

6.4 System Overview

In this section, the vehicle system has presented with more detail including the electronic components, the system was designed for a restraint combination of motors and elevons to control it, in its whole flight envelope. Thus the vehicle was predefined for a certain electronic components, since the development of the tail-sitter, that has proposed in this work, it is not concluded because of some factors, we have integrated the pixhawk autopilot electronic to verify the control that has proposed lately. As it can be shown the proposed design does not require additional hardware for the transition maneuver, as presented the tilt rotors in [49], it is other type of configuration transition maneuver. This type of configuration has a high cost and complexity mechanical system while in the figuration proposed in this work, allows having a low cost and complexity mechanical system, but its maneuver transition, it is more complicated than the tilt-rotors.

Actuators

The system is constituted of a wing with four brushless motors and two servo for actuating the elevons. All actuators are directly connected to Pulse Width Modulation (PWM)output channels of the autopilot. The PWM signal used is the standard protocol for commanding actuators in RC transmitter application which enables the use of low cost off-the-shelf motors controllers and servos. The standard frequency of the PWM command signal in RC transmitter application from px4 is 50HZ for controlling the servos this frequency is sufficient but for motors controller is not sufficient, as RC motor controllers in px accept frequency up to 400Hz thus the motor controllers are updated at this rate.

Wing

It is also included an electronic box, which has divided in two parts, one for the batteries and the other one for the electronic components as illustrated in the figure 4.8, whole the system has mass $m = 1kg$. The main wing of the system is a $1m$ span and $0.1625m$ average chord platform, the system uses four propellers for its propulsion ($208\times114mm$), (8×4.5)

Avionics

The vehicle avionics are based on the pixhawk, and several sensors that integrated in the hardware have been used in order to estimate the vehicle posture and enable its automatic control, such as: The Inertial Measurement Unit (IMU) with integrated 3 axis accelerometer and the gyroscope to measure the accelerations and the angular

velocities which are acting on the vehicle, a magnetometer to measure the magnetic flux. a GPS module for position updating, a barometer to asses the atmospheric pressure and a differential pressure sensor to calculate the velocity of the air-stream. All the information gathered from the sensors is then used to estimate the pose, using the Extended Kalman Filter (EKF).

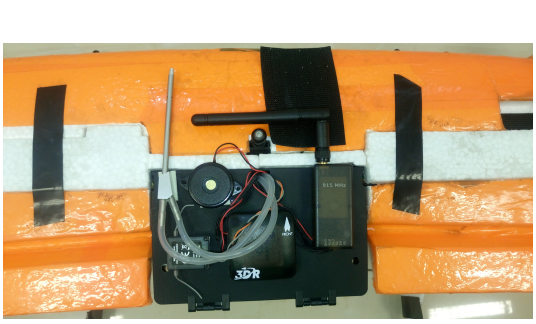

(a) Peripherals Connection

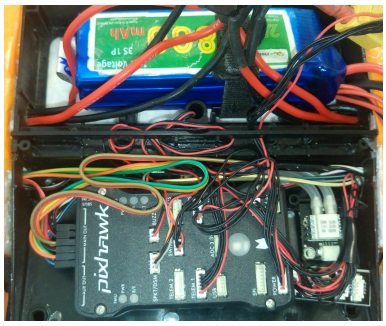

(b) Electronic Box

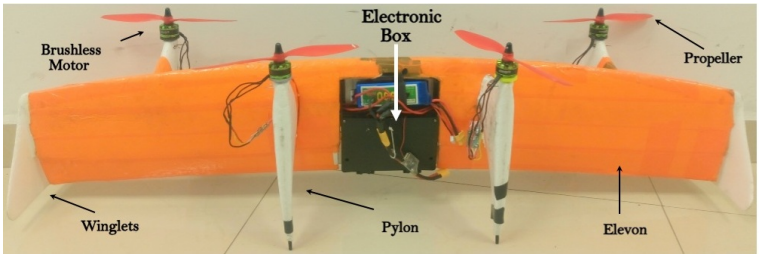

(c) Hardware Configuration

Fig. 6.8: System Overview.

Flight Envelope

In the following figure, the typical flight envelope has shown, where the vehicle has for mission, hover-to-level and vice versa flight. When the vehicle is about to take off, the propellers point upwards which allows the tail-sitter to hover. Subsequently, the transition gets triggered and the whole vehicle pitches to 90^o forward to get the hover-

to-level flight, the lift is now produced by the aerodynamic effects of the wing instead of the propellers, which allows decreasing the power consumption, once the vehicles reaches the desired landing point, now pitching up 90^o and then the vehicle is getting the level-to-hover flight. An illustration of the flight envelope of the tail-sitter is shown the following figure.

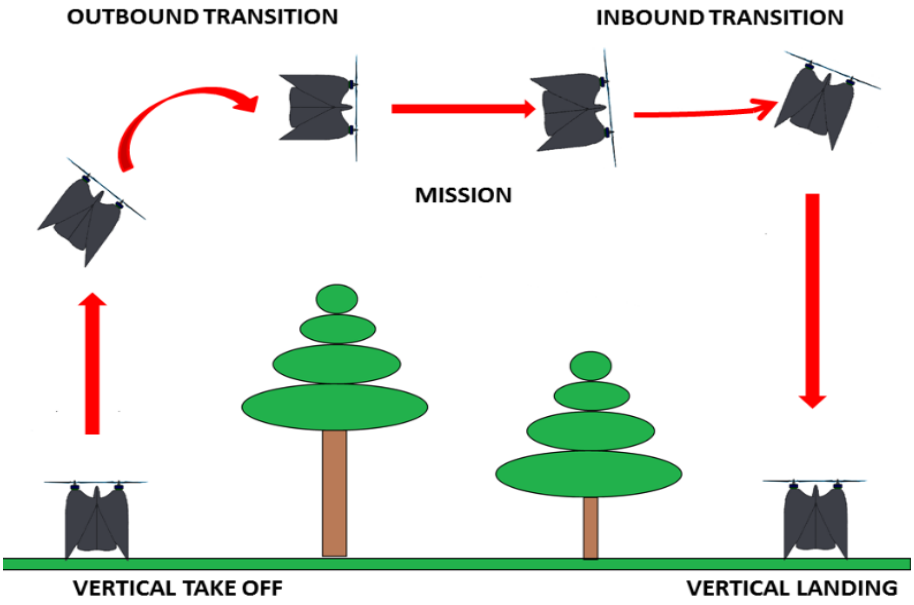

Fig. 6.9: Flight Envelope

Chapter 7

Conclusion

The aim of this thesis was to obtain the 6-DOF model and longitudinal dynamics of a Quad-Rotor Tail-sitter UAV using quaternion approaches, designed control laws to stabilize the vehicle in its three phases and implemented the control laws on a platform using autopilot px4.

In this thesis, we have investigated about of different UAVs classifications especially on convertibles UAVs of which our work is focused on the tail-sitter. And for modeling, the quaternion approches have been studied, where the 6-DOF and the Longitudinal Dynamics are obtained, we also presented an Airfoil Analysis by comparing a 4-digits series airfoils with a 4-digits Modified series airfoils it is worth to clarify that we have also studied the Aerodynamic forces, The Airfoils analysis was done to help us build a suitable prototype, which was built using composite materials and finally we have presented the control designs using backstepping approaches, as Backstepping deals explicitly with stability, through the construction of a Lyapunov function for the closed loop system along with the construction of the control law itself.

It is important to illustrate that, as our model is completely a nonlinear system for this reason we have used backstepping designs which is focused on utilizing useful nonlinearities rather than cancelling them, the resulting closed loop systems are not linear, this means we have more information about vehicle and that the aircraft response to the pilot inputs will not be independent of the angle of attack.

Bibliography

[1] J. B. Kuipers, *Quaternions and rotation sequences*, vol. 66. Princeton university press Princeton, 1999. xi, 13, 17

[2] B. R. W. Beard, T. W. McLain, D. B. Nelson, D. Kingston, and D. Johanson, "Decentralized cooperative aerial surveillance using fixed-wing miniature uavs," *Proceedings of the IEEE*, vol. 94, no. 7, pp. 1306–1324, 2006. 1

[3] D. Viegas, M. Cruz, L. Ribeiro, A. Silva, A. Ollero, B. Arrue, R. Dios, F. Gómez-Rodríguez, L. Merino, A. Miranda, *et al.*, "Gestosa fire spread experiments.," in *Forest fire research and wildland fire safety: Proceedings of IV International Conference on Forest Fire Research 2002 Wildland Fire Safety Summit, Luso, Coimbra, Portugal, 18-23 November 2002.*, Millpress Science Publishers, 2002. 1

[4] P. Doherty and P. Rudol, "A uav search and rescue scenario with human body detection and geolocalization," in *AI 2007: Advances in Artificial Intelligence*, pp. 1–13, Springer, 2007. 1

[5] E. Feron and E. N. Johnson, "Aerial robotics," in *Springer Handbook of Robotics*, pp. 1009–1029, Springer, 2008. 1

[6] R. Austin, *Unmanned aircraft systems: UAVS design, development and deployment*, vol. 54. John Wiley & Sons, 2011. 2

[7] J. G. Leishman, *Principles of Helicopter Aerodynamics with CD Extra*. Cambridge university press, 2006. 5, 6, 8

[8] T. Ostermann, J. Holsten, Y. Dobrev, and D. Moormann, "Control concept of a tiltwing uav during low speed manoeuvring," in *Proceeding of the 28th International Congress of the Aeronautical Sciences: ICAS Brisbane, Australia*, 2012. 5

[9] M. Maisal, D. Giulianetti, and D. Dugan, "The history of the xv-15 tilt rotor research aircraft," tech. rep., NASA SP-2000-4517, 2000. 6

[10] J. V. Hogge, "Development of a miniature vtol tail-sitter unmanned aerial vehicle," 2008. 7

[11] J. Guerrero and R. Lozano, *Flight formation control*. John Wiley & Sons, 2012. 8, 25

[12] A. S. Saeed, A. B. Younes, S. Islam, J. Dias, L. Seneviratne, and G. Cai, "A review on the platform design, dynamic modeling and control of hybrid uavs," in *Unmanned Aircraft Systems (ICUAS), 2015 International Conference on*, pp. 806–815, IEEE, 2015. 8

[13] H. L. Tinger, "Analysis and application of aircraft departure prediction criteria to the av-8b harrier ii," in *AIAA Atmospheric Flight Mechanics Conference, Technical Papers, Monterey, CA*, vol. 17, p. 19, 1987. 8

[14] H. Powrie and A. Novis, "Gas path debris monitoring for f-35 joint strike fighter propulsion system phm," in *Aerospace Conference, 2006 IEEE*, pp. 8–pp, IEEE, 2006. 8

[15] B. Norton, *Bell Boeing V-22 Osprey: Tiltrotor Tactical Transport*. Aerofax, 2004. 8

[16] R. H. Stone, "Control architecture for a tail-sitter unmanned air vehicle," in *Control Conference, 2004. 5th Asian*, vol. 2, pp. 736–744, IEEE, 2004. 9

[17] L. Bridgman, L. Howard-Flanders, F. T. Jane, and C. G. Grey, *Jane's all the world's aircraft*. McGraw-Hill, 1909. 9

[18] D. Taylor, M. Ol, and T. Cord, "Skytote advanced cargo delivery system," in *2003 AIAA/ICAS International Air and Space Symposium and Exposition: The Next 100 Years*, 2003. 9

[19] P. Sinha, P. Esden-Tempski, C. Forrette, J. K. Gibboney, G. M. Horn, *et al.*, "Versatile, modular, extensible vtol aerial platform with autonomous flight mode transitions," in *Aerospace Conference, 2012 IEEE*, pp. 1–17, IEEE, 2012. 11, 42, 46

[20] Y. Yang, "Spacecraft attitude determination and control: Quaternion based method," *Annual Reviews in Control*, vol. 36, no. 2, pp. 198–219, 2012. 13, 15, 20, 22

[21] E. Fresk and G. Nikolakopoulos, "Full quaternion based attitude control for a quadrotor," in *Control Conference (ECC), 2013 European*, pp. 3864–3869, IEEE, 2013. 21

[22] J. Diebel, "Representing attitude: Euler angles, unit quaternions, and rotation vectors," *Matrix*, vol. 58, pp. 15–16, 2006. 22

[23] R. Schlanbusch, A. Loria, and P. J. Nicklasson, "On the stability and stabilization of quaternion equilibria of rigid bodies," *Automatica*, vol. 48, no. 12, pp. 3135–3141, 2012. 24

[24] A. Loría and E. Panteley, "6 stability, told by its developers," in *Advanced topics in control systems theory*, pp. 199–258, Springer, 2006. 24

[25] W. Hahn and A. P. Baartz, *Stability of motion*, vol. 138. Springer, 1967. 24

[26] J.-Y. Wen and K. Kreutz-Delgado, "The attitude control problem," *Automatic Control, IEEE Transactions on*, vol. 36, no. 10, pp. 1148–1162, 1991. 24

[27] J. D. Boškovic, S.-M. Li, and R. K. Mehra, "Robust adaptive variable structure control of spacecraft under control input saturation," *Journal of Guidance, Control, and Dynamics*, vol. 24, no. 1, pp. 14–22, 2001. 24

[28] R. J. Wallsgrove and M. R. Akella, "Globally stabilizing saturated attitude control in the presence of bounded unknown disturbances," *Journal of Guidance, Control, and Dynamics*, vol. 28, no. 5, pp. 957–963, 2005. 24

[29] R. A. Paielli and R. E. Bach, "Attitude control with realization of linear error dynamics," *Journal of Guidance, Control, and Dynamics*, vol. 16, no. 1, pp. 182–189, 1993. 24

[30] B. Wie, *Space vehicle dynamics and control*. Aiaa, 1998. 24

[31] R. Kristiansen, P. J. Nicklasson, and J. T. Gravdahl, "Quaternion-based backstepping control of relative attitude in a spacecraft formation," in *Decision and Control, 2006 45th IEEE Conference on*, pp. 5724–5729, IEEE, 2006. 24

[32] H. Goldstein, *Classical mechanics*. Pearson Education India, 1965. 25

[33] E. Y. Gu, *A journey from robot to digital human: mathematical principles and applications with MATLAB programming*, vol. 1. Springer Science & Business Media, 2013. 25

[34] R. W. Beard and T. W. McLain, *Small unmanned aircraft: Theory and practice*. Princeton university press, 2012. 25

[35] C. L. Ladson, A. S. Hill, and D. Sproles, *Computer program to obtain ordinates for NACA airfoils*, vol. 4741. National Aeronautics and Space Administration, Langley Research Center, 1996. 35

[36] C. L. Ladson and C. W. Brooks, "Development of a computer program to obtain ordinates for naca-6 and 6 a-series airfoils," 1974. 35

[37] J. Stack and A. E. Von Doenhoff, *Tests of 16 related airfoils at high speeds*. NACA, 1934. 37, 38, 39

[38] M.-D. Hua, T. Hamel, P. Morin, and C. Samson, "A control approach for thrust-propelled underactuated vehicles and its application to vtol drones," *Automatic Control, IEEE Transactions on*, vol. 54, no. 8, pp. 1837–1853, 2009. 42

[39] D. Pucci, T. Hamel, P. Morin, and C. Samson, "Modeling for control of symmetric aerial vehicles subjected to aerodynamic forces," *arXiv preprint arXiv:1212.1629*, 2012. 44, 45

[40] D. Pucci, T. Hamel, P. Morin, and C. Samson, "Nonlinear control of pvtol vehicles subjected to drag and lift," in *Decision and Control and European Control Conference (CDC-ECC), 2011 50th IEEE Conference on*, pp. 6177–6183, IEEE, 2011. 44

[41] B. Efron and B. Efron, *The jackknife, the bootstrap and other resampling plans*, vol. 38. SIAM, 1982. 44

[42] J. D. Anderson Jr, *Fundamentals of aerodynamics*. Tata McGraw-Hill Education, 1985. 44

[43] J. N. Reddy, "Mechanics of laminated composite plates- theory and analysis(book)," *Boca Raton, FL: CRC Press, 1997.*, 1997. 47

[44] S. Mazumdar, *Composites manufacturing: materials, product, and process engineering*. CrC press, 2001. 48

[45] T. Turgut, "Manufacturing and structural analysis of a lightweight sandwich composite uav wing," *Middle East Technical University Thesis of MS*, 2007. 48

[46] I. M. Daniel, O. Ishai, I. M. Daniel, and I. Daniel, *Engineering mechanics of composite materials*, vol. 3. Oxford university press New York, 1994. 48

[47] L. Meier, P. Tanskanen, F. Fraundorfer, and M. Pollefeys, "Pixhawk: A system for autonomous flight using onboard computer vision," in *Robotics and automation (ICRA), 2011 IEEE international conference on*, pp. 2992–2997, IEEE, 2011. 56

[48] L. Meier, P. Tanskanen, L. Heng, G. H. Lee, F. Fraundorfer, and M. Pollefeys, "Pixhawk: A micro aerial vehicle design for autonomous flight using onboard computer vision," *Autonomous Robots*, vol. 33, no. 1-2, pp. 21–39, 2012. 56

[49] G. Flores and R. Lozano, "A nonlinear control law for hover to level flight for the quad tilt-rotor uav," in *World Congress*, vol. 19, pp. 11055–11059, 2014. 57

[50] D. McLean, "Automatic flight control systems(book)," *Englewood Cliffs, NJ, Prentice Hall, 1990, 606*, 1990. 62

[51] M. Krstic, P. V. Kokotovic, and I. Kanellakopoulos, *Nonlinear and adaptive control design*. John Wiley & Sons, Inc., 1995. 62

[52] T. C. Kiat, H. Son, and P. Y. Chai, "Uav flight path control using contraction-based back-stepping control," *Open Journal of Applied Sciences*, vol. 3, no. 02, p. 65, 2013. 62

[53] L. Chrif, Z. M. Kada, and T. Mohamed, "Flight-path tracking control of an aircraft using backstepping controller," *TELKOMNIKA Indonesian Journal of Electrical Engineering*, vol. 15, no. 2, pp. 270–276, 2015. 62

[54] R. F. Stengel, *Flight dynamics*. Princeton University Press, 2015. 63

[55] B. L. Stevens, F. L. Lewis, and E. N. Johnson, *Aircraft Control and Simulation: Dynamics, Controls Design, and Autonomous Systems*. John Wiley & Sons, 2015. 63, 81

[56] F. Gavilan, J. A. Acosta, and R. Vazquez, "Control of the longitudinal flight dynamics of an uav using adaptive backstepping," in *IFAC World Congress*, 2011. 64

[57] O. Härkegård and T. Glad, "Flight control design using backstepping," 2000. 65

[58] M. Krstic and P. Kokotovic, "Lean backstepping design for a jet engine compressor model," in *Control Applications, 1995., Proceedings of the 4th IEEE Conference on*, pp. 1047–1052, IEEE, 1995. 68

[59] A. Abdessameud and A. Tayebi, *Motion Coordination for VTOL Unmanned Aerial Vehicles: Attitude Synchronisation and Formation Control*. Springer Science & Business Media, 2013. 72, 94

[60] M. D. Shuster, "A survey of attitude representations," *Navigation*, vol. 8, no. 9, pp. 439–517, 1993. 76

[61] S. Zhao, W. Dong, and J. A. Farrell, "Quaternion-based trajectory tracking control of vtol-uavs using command filtered backstepping," in *American Control Conference (ACC), 2013*, pp. 1018–1023, IEEE, 2013. 82

[62] C. G. Mayhew, R. G. Sanfelice, and A. R. Teel, "Quaternion-based hybrid control for robust global attitude tracking," *Automatic Control, IEEE Transactions on*, vol. 56, no. 11, pp. 2555–2566, 2011. 83

[63] C. G. Mayhew, R. G. Sanfelice, and A. R. Teel, "Robust global asymptotic attitude stabilization of a rigid body by quaternion-based hybrid feedback," in *Decision and Control, 2009 held jointly with the 2009 28th Chinese Control Conference. CDC/CCC 2009. Proceedings of the 48th IEEE Conference on*, pp. 2522–2527, IEEE, 2009. 87

[64] N. B. Knoebel, "Adaptive quaternion control for a miniature tailsitter uav," 2007. 88